University of Saskatchewan
Subatomic Physics Internal Report

SPIR 142

Blowfish Gain Analysis for 2008 Runs

Rob Pywell and Ward Wurtz

March 26, 2008

Abstract

This document describes an investigation of the gain determination procedure for the *Blowfish* BC-505 cells. A detailed investigation of the resulting gains brings to light a number of effects that require further study.

Contents

1 Introduction

This document describes an investigation the gains for the *Blowfish* cells runs during the June-July and September-October 2008 running periods. This includes an analysis of the gain monitoring system which uses the LED and fiber optic flasher.

2 Gain Calibration

The first priority is to determine the gains of each BC-505 cell as measured in dedicated calibration runs using a radioactive source. The gain relates ADC channel number to light output in equivalent electron energy units [1, 2]. The gain for a particular cell i is define by

$$g_i = E_{ee}/A_i \tag{1}$$

where E_{ee} is the equivalent electron energy of some feature in the light output spectrum and A_i is the ADC channel number of that feature.

Two gamma ray sources were used for these calibrations: a ^{232}Th source which has a gamma ray of energy 2.614 MeV, and a AmBe source which has a gamma ray of energy 4.430 MeV. In addition, the room background contains Thorium so the 2.614 MeV gamma ray is visible in background spectra as well.

Because BC-505 does not have a prominent photoelectric peak in response to gamma rays we must rely on the Compton edge for the energy calibration. The Compton edge is found by fitting a curve to the endpoint of the light output spectrum. This curve is then examined to find the inflection point (where the slope has maximum magnitude). The fitting algorithm, as implemented by the routing "fitedge.c" (which can be called from *Lucid* [3]) first searches a smoothed version of the spectrum for an edge. The region around this found edge is then fitted with a curve to find the inflection point. Before now the data that was fitted was the smoothed spectrum and the curve used in the fit was based on the error function. While this gave pretty good results some anomalies in the results to be discussed later prompted a closer look at the fitting procedure. In particular there was concern that the smoothing process might distort the shape of the fitted curve and affect the results differently for an edge at a high channel number compared to one at low channel number.

Therefore the algorithm was improved in the following ways. A smoothed spectrum was still used to find the initial edge position, but some improvements were made to make this edge finding more robust in the face of poor statistics. Once an edge was found the curve fitting was done directly to the unsmoothed data, thus removing any bias introduced by the smoothing process. The curve that is fitted to the data was changed to one side of a Gaussian with a linear background. This is a more realistic shape for the endpoint since the Compton edge seen in the light output spectrum would be a sharp edge convoluted with the detector resolution. The fitting function is then

$$f(x) = a_0 + a_1 x + a_2 \exp(-(x - a_3)^2/2a_4^2). \tag{2}$$

The inflection point is then determined from

$$E_{InflectionPoint} = a_3 + a_4 \tag{3}$$

since the one standard deviation point in a Gaussian is also an inflection point. The smoothed spectrum was used to find an initial guess for $E_{InflectionPoint}$ by finding the position with maximum negative slope. As well the smoothed spectrum provided initial guesses for a_2 and a_3 by finding the position of maximum counts below the position with maximum slope. After an initial fit to the data near the initial guess for the inflection point, a second fit, restricted to the range from $a_3 - 0.15a_4$ to $a_3 + 3a_4$ was made to refine the fit.

The relationship between the inflection point and the actual Compton edge was then examined using a GEANT4 [4] simulation of *Blowfish*. In the simulation gamma rays of single energy were released from the center of *Blowfish* and light output spectra were recorded for the *Blowfish* cells. In the analysis of both the real data and the simulated data only cell hit multiplicities of one were used to the fill the light output spectra for end-point finding. The real ADC data were pedestal corrected. The same fitting procedure was applied to both the real and simulated data to determine the inflection point. Figure 1 shows an example of the fit for the 4.430 MeV gamma ray from the AmBe source and figure 2 shows an example of the fit for the 2.614 MeV gamma ray from the Thorium source In the plot the energy scale of the real data has been scaled so that its inflection point matches that of the simulated data. (This scaling factor is of course the gain.) Also, the counts for the simulation have been scaled so that the integral of both spectra match in the region of the endpoint. Because of this scaling the excellent agreement between the simulation and the data merely shows that we have used a correct value for the energy resolution in the simulation. This gives us confidence that we can use the simulation to determine the relationship between the inflection point and the Compton edge energy. Also shown in figures 1 and 2 are lines showing the inflection point and the true Compton energy.

The GEANT4 simulation was used to determine the fitted inflection point for a range of photon energies. The difference between the fitted inflection points and the true Compton edge energy are plotted in figure 3. The average deviation is

$$\Delta E_c = E_{InflectionPoint} - E_{ComptonEdge} = 0.053 \pm 0.001\text{MeV} \tag{4}$$

If A_i is the ADC channel number of the fitted inflection point when a gamma source with a Compton edge energy of E_c is placed near *Blowfish* then the gain for cell i may be calculated from

$$g_i = \left(E_c + \Delta E_c\right)/A_i \tag{5}$$

In the analysis that follows the BC-505 cell gains are all calculated using this procedure.

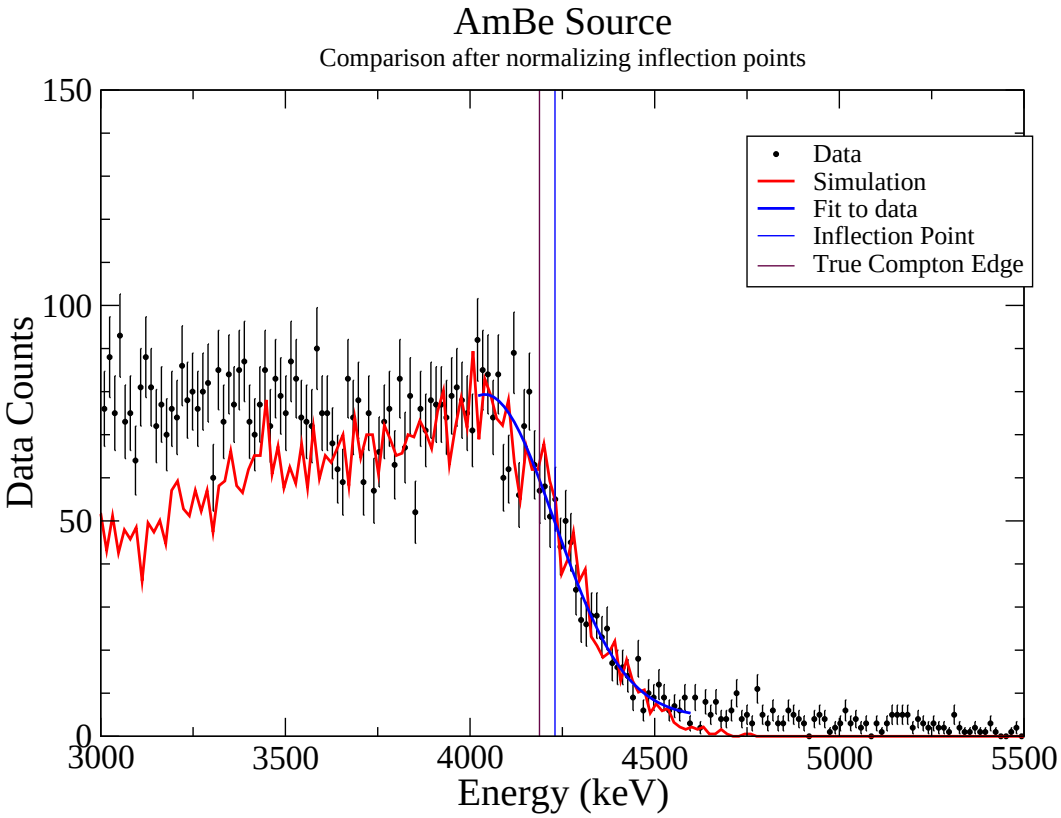

Figure 1: The Compton Edge for the 4.430 MeV gamma ray from the AmBe source. The data for a particular cell is compared to the GEANT4 simulation. The energy scale of the data has been scaled so that the inflection points found from the data and the simulation match. The counts of the simulation have been scaled so that the integral of the spectra in the region of the end-point match. Also shown is the position of the inflection point and the true Compton edge energy (at 4.188 MeV). The simulation underestimates the data at energies below 3700 keV because of gammas present in the AmBe spectrum that are not included in the simulation.

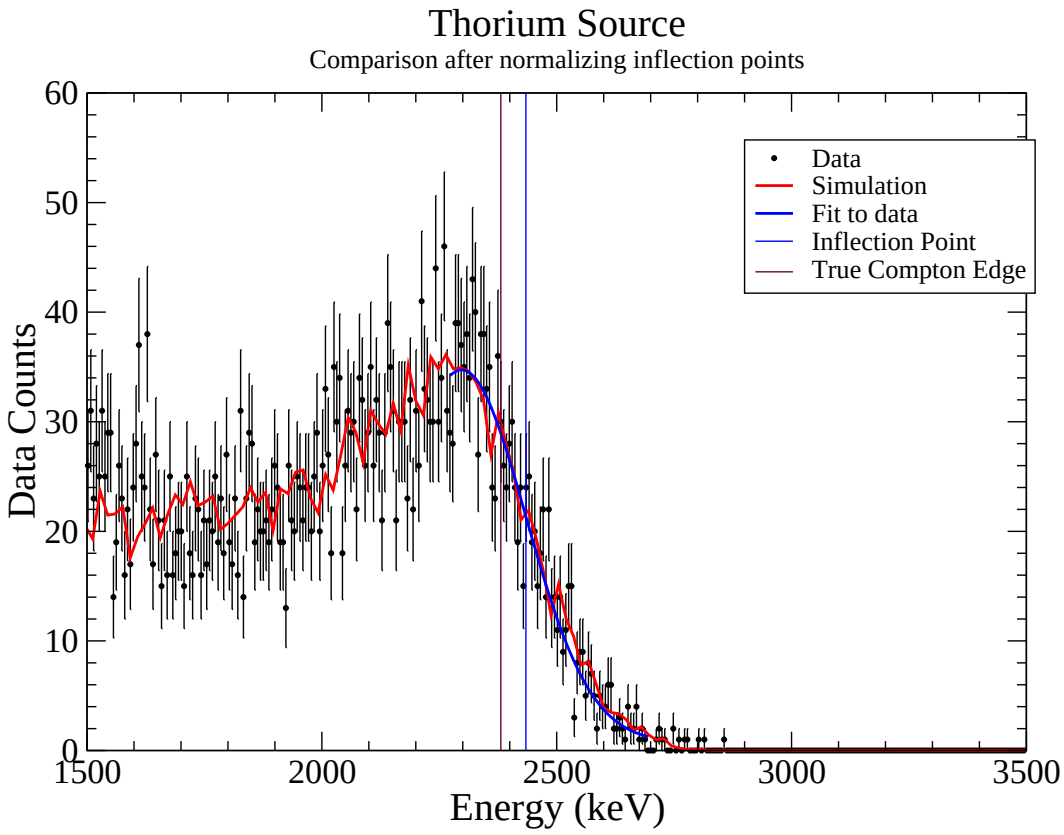

Figure 2: The Compton Edge for the 2.614 MeV gamma ray from the Thorium source. The data for a particular cell is compared to the GEANT4 simulation. The energy scale of the data has been scaled so that the inflection points found from the data and the simulation match. The counts of the simulation have been scaled so that the integral of the spectra in the region of the end-point match. Also shown is the position of the inflection point and the true Compton edge energy (at 2.381 MeV).

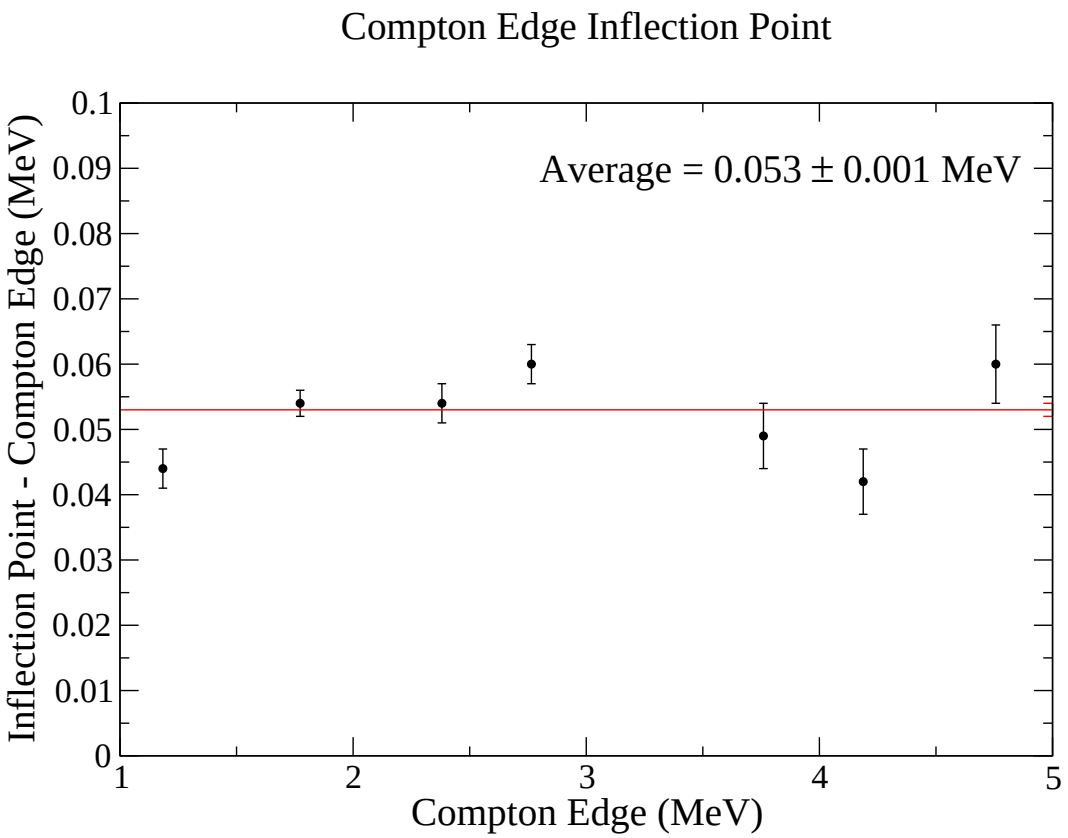

Figure 3: The difference between the fitted inflection point and the Compton edge energy is plotted as a function of Compton edge energy.

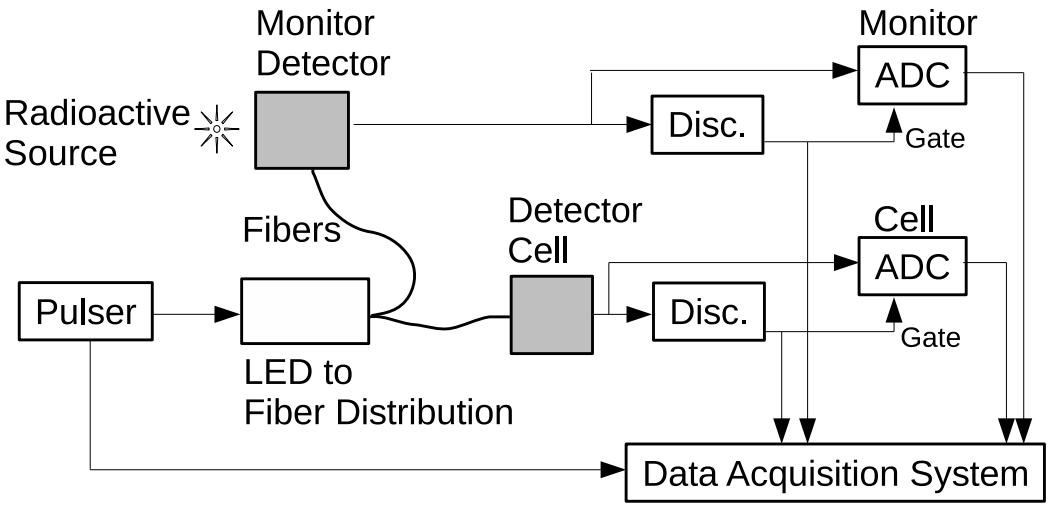

Figure 4: Conceptual schematic of the gain monitoring system.

3 Gain Monitoring System

We will now examine the performance of the LED flasher and fiber optic gain monitoring system of *Blowfish*[5].

3.1 Gain Tracking Principles

The concept of the gain monitoring system in illustrated in figure 4. A pulser will fire a single LED whose light will be captured by a fiber optic bundle. Individual fibers in the bundle take the light to the neutron detector cells in *Blowfish* (only one is illustrated in the drawing). As well, a fiber in the same bundle takes light to a separate monitor detector. A radioactive source is also present near the monitor detector.

During a calibration run the gain, g_i, of each cell can be determined as described in section 2 using equation 5.

At the same time data is recorded from the LED flasher. If an amount of light L is produced by the LED, and a certain fraction x_i of it reaches cell i, then the peak due to the LED flasher will appear in channel

$$A_{Fi} = x_i L / g_i \tag{6}$$

If a feature from the radioactive source near the monitor detector m with light output E_M is observed to be at ADC channel A_m then the gain for monitor m is determined by

$$g_m = E_M / A_m. \tag{7}$$

If the fraction of the LED light L reaching the monitor detector is x_m, then the peak due to the LED flasher in the monitor histogram will appear in channel

$$A_{Fm} = x_m L / g_m \tag{8}$$

All the quantities here are known or measured except L, x_i and x_m. Combining equations 6 and 8 the following ratio for each cell can be calculated

$$R_i = \frac{x_i}{x_m} = \frac{g_i}{g_m}\frac{A_{Fi}}{A_{Fm}} \tag{9}$$

During a later data taking run the light produced by the LED may have changed, the gains of the cells may have changed, and the gain of the monitor detectors may have changed. We denote these changed quantities by L', g'_i and g'_m respectively. If the source feature in the monitor spectrum appears at channel A'_m then the monitor gain can be determined from

$$g'_m = E_M/A'_m. \tag{10}$$

We allow the fraction of the LED light reaching cell i to now be x'_i and the fraction of the LED light reaching the monitor detector m to now be x'_m. Then the flasher peak will appear in the cell spectrum at channel

$$A'_{Fi} = x'_i L'/g'_i \tag{11}$$

and in the monitor spectrum at channel

$$A'_{Fm} = x'_m L'/g'_m \tag{12}$$

Combining equations 11 and 12 we solve for the required cell gain

$$g'_i = g'_m \frac{A'_{Fm}}{A'_{Fi}}\frac{x'_i}{x'_m} = g'_m \frac{A'_{Fm}}{A'_{Fi}} R'_i \tag{13}$$

where $R'_i = x'_i/x'_m$.

The gain tracking system relies on being able to make the assumption that $R'_i = R_i$. This is a justifiable assumption provided there are no serious mechanical changes between the two runs that could change the light transport efficiency through the fibers going to the *Blowfish* cells or to the monitor detectors. The required cell gain in the data taking run is then given by

$$g'_i = g'_m R_i \frac{A'_{Fm}}{A'_{Fi}}. \tag{14}$$

3.2 Light Transport Efficiency

The first thing to test is the $R'_i = R_i$ assumption noted above. This can only be done for gain calibration runs where we have both g_i and g_m determined.

During the June/July 2008 running period a problem with the data acquisition trigger electronics prevented the flasher system from being used during normal data taking. However flasher data was recorded during calibration runs. The trigger electronics was completely rebuilt before the September/October 2008 running period. Therefore the gain monitoring system was functional for this period except for the fact that the BNC-555 pulser driving the LED flasher would intermittently quit.

Table 1: Calibration runs for the June/July 2008 running period. Run numbers in brackets indicate that the data for the calibration run listed in the line above is actually a concatenation of the run number range in the brackets.

Run Number	Source	Nominal Cell Gain (keV/ch)	Date/Time	Flasher Present
163	Thorium	1.00	June 30, 2008 0748	Yes
(162-163)				
164	Background	1.00	June 30, 2008 0810	Yes
196	Thorium	1.00	June 30, 2008 1737	Yes
210	Thorium	1.00	June 30, 2008 2152	Yes
228	Thorium	1.00	July 1, 2008 1205	No
284	Thorium	1.00	July 1, 2008 2140	Yes
(283-184)				
297	Thorium	1.00	July 2, 2008 0825	Yes
(296-297)				
298	Background	1.00	July 2, 2008 0903	Yes
307	Thorium	1.00	July 2, 2008 1327	Yes
321	Thorium	1.00	July 2, 2008 1722	Yes
333	Thorium	1.00	July 2, 2008 2350	Yes
347	Thorium	1.40	July 3, 2008 0901	Yes
(345-347)				
362	Thorium	1.40	July 3, 2008 1412	Yes
385	Thorium	1.40	July 3, 2008 1759	Yes
(378-385)				
397	Thorium	1.40	July 3, 2008 2352	No
398	Thorium	1.40	July 4, 2008 0012	No
399	AmBe	1.40	July 4, 2008 0023	No
400	AmBe	1.40	July 4, 2008 0037	No
401	Background	1.40	July 4, 2008 0053	No

Table 2: Calibration runs for the September/October 2008 running period.

Run Number	Source	Nominal Cell Gain (keV/ch)	Date/Time	Flasher Present
606	AmBe	1.67	Sept 24, 2008 0837	Yes
685	AmBe	1.67	Sept 25, 2008 0921	No
717	AmBe	1.67	Sept 25, 2008 2154	Yes
718	AmBe	1.67	Sept 26, 2008 0800	Yes
735	AmBe	1.67	Sept 26, 2008 2155	Yes
802	AmBe	3.33	Sept 29, 2008 0931	No
832	AmBe	3.33	Sept 29, 2008 2157	Yes
833	AmBe	3.33	Sept 30, 2008 0812	No
866	AmBe	3.33	Sept 30, 2008 2151	Yes
876	AmBe	3.33	Oct 1, 2008 0914	Yes
903	AmBe	3.33	Oct 1, 2008 2154	Yes
907	Background	3.33	Oct 1, 2008 2215	Yes
908	AmBe	3.33	Oct 2, 2008 0821	Yes
936	AmBe	3.33	Oct 2, 2008 2165	Yes
944	AmBe	5.00	Oct 3, 2008 0828	Yes
980	AmBe	5.00	Oct 3, 2008 2200	Yes

Tables 1 and 2 list the gain calibration runs for the June/July and September/October 2008 running periods and whether or not flasher data was present. In general calibration data were recorded at the beginning and end of each data-taking day.

The value of R_i was calculated using equation 9 for each cell in all runs for which flasher data was present. (Note that care must be taken in this calculation to pair each cell with its appropriate LED/Monitor combination.) To get a sense of how R_i varied as a function of time the value of R_i divided by the average value of R_i for a whole run period, is plotted as a function of time. This is done for eight cells in figure 5 for the September/October run period and for the same eight cells in figure 6 for the June/July run period. Only calibrations performed using a single source (Thorium for June/July and AmBe for September/October) are included in these figures. It can be seen that the value of R_i for each cell varies by less than a few percent over the whole September/October running period. However for the June/July run period there are large changes especially in the first two days of running. This corresponds to the time when many changes were being made while the system was being debugged.

In practice we will only need to track the gain over the course of an individual day's running. Therefore we compare, for all cells, the value of R_i determined from a particular calibration run (usually at the end of a day) to its value determined from an earlier calibration run (usually at the beginning of the same day). These ratios are displayed in figures 7-12. In general, it can be seen that the value of R_i varies by less than a few percent from one calibration run to the next. This would suggest that the gains for runs in between calibration

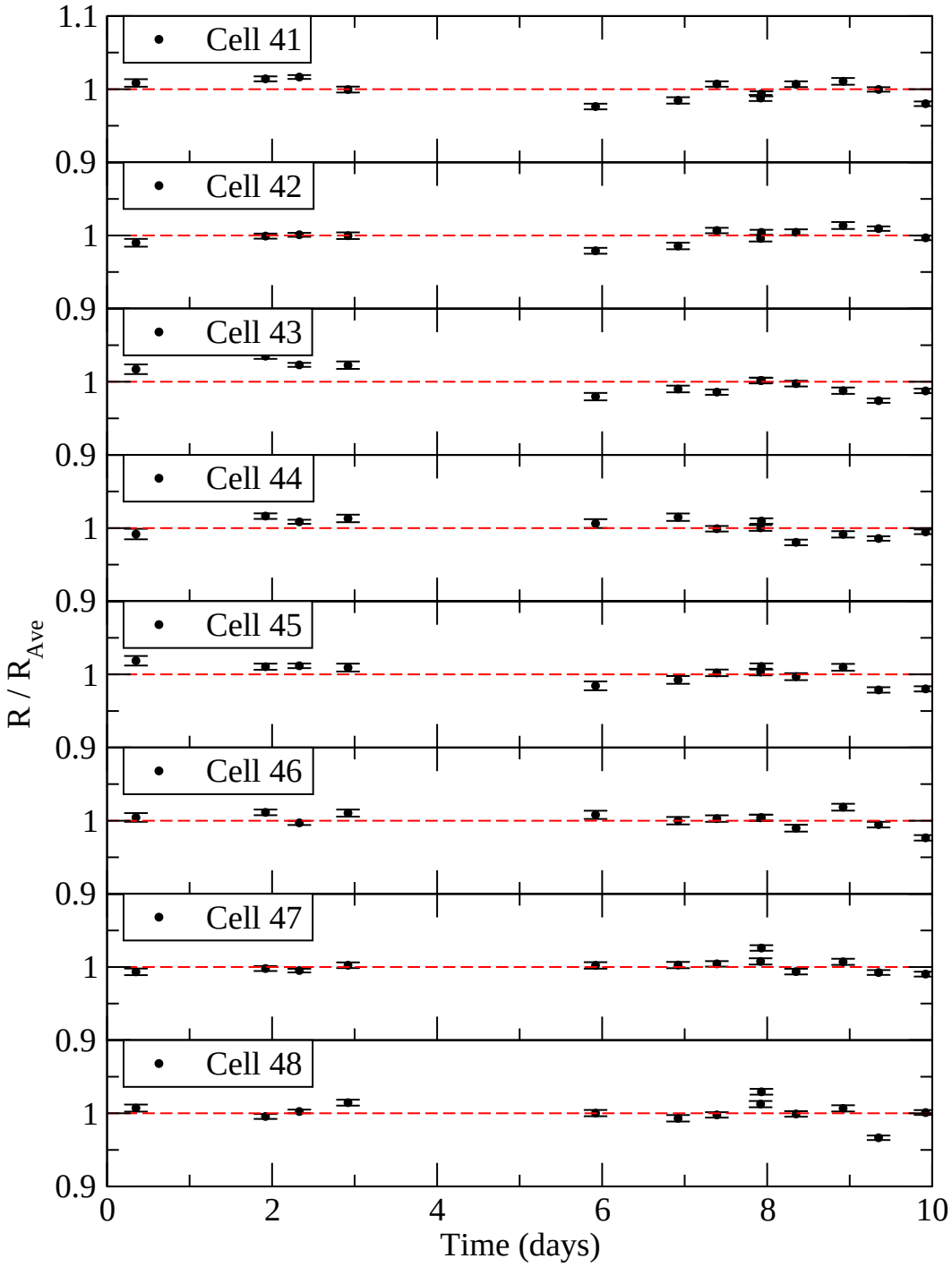

Figure 5: The value of R_i divided by the average value of R_i for eight cells is plotted as a function of time for the September/October run period.

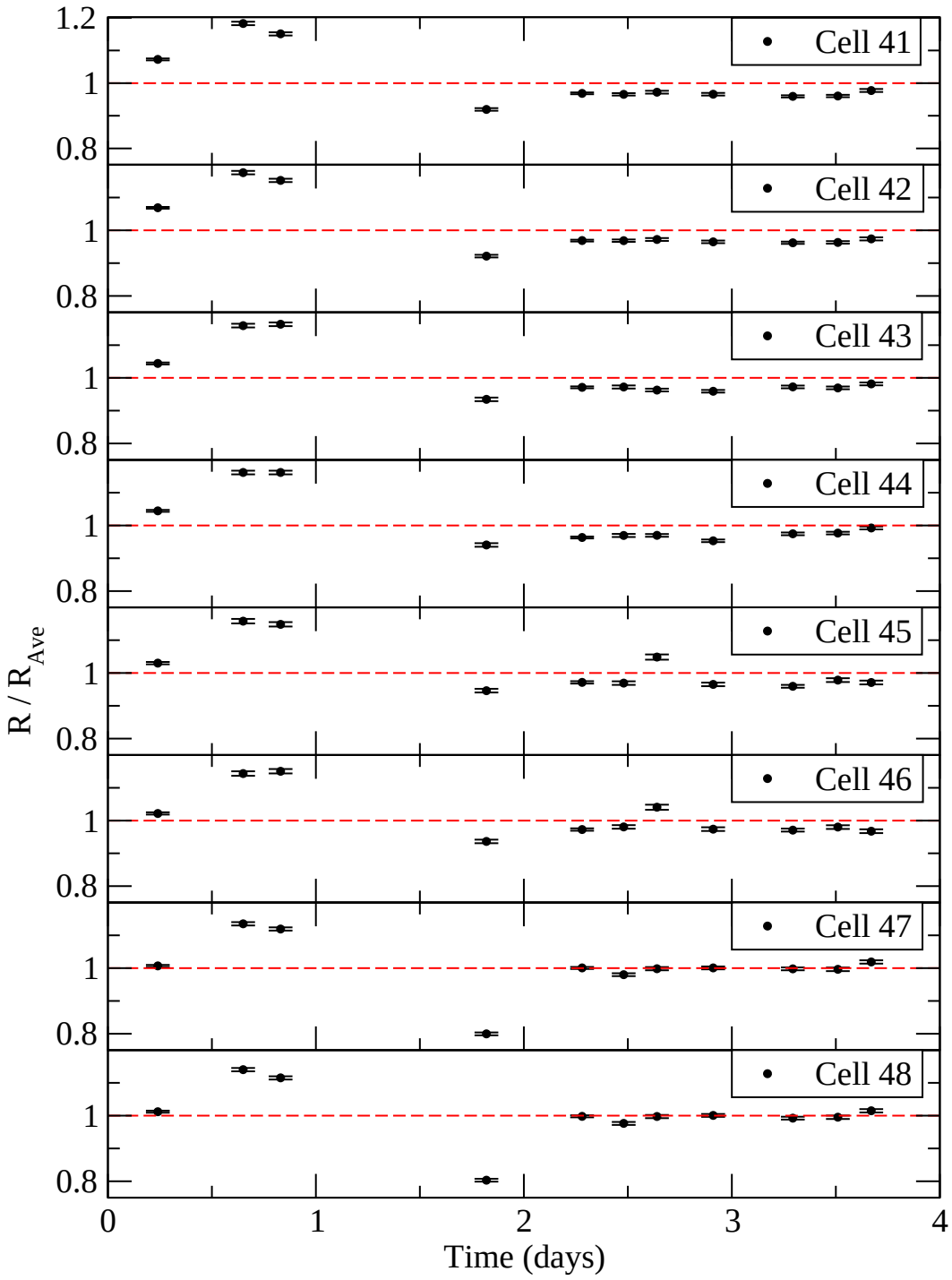

Figure 6: The value of R_i divided by the average value of R_i for eight cells is plotted as a function of time for the June/July run period.

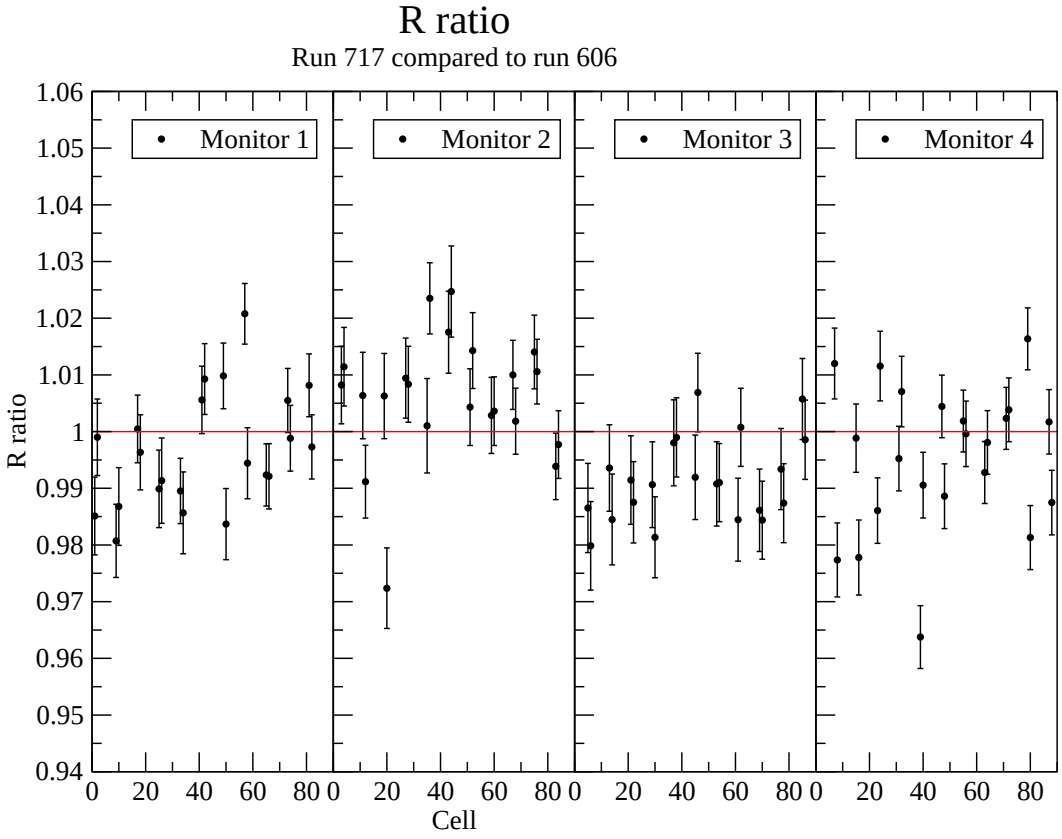

Figure 7: The value of R_i for a particular run divided by the value of R_i for an earlier run. The ratios are plotted for all cells and are subdivided according to the LED/Monitor to which the cell is linked.

runs can be tracked to within a few percent.

In many cases it can be seen that the value of R_i', calculated from a later calibration run, for cells associated with a given LED/Monitor, scatter around the value of R_i calculated from the earlier run in a manner consistent with the uncertainties. However in other cases there appears to be a systematic shift in the value of R_i' compared to R_i for cells associated with a particular LED/Monitor. This would indicate that there has been a change in x_m, the fraction of light transported along the fiber going to that monitor detector. This could well be possible. The monitor detectors are mounted on the *Blowfish* frame while the LED boxes are mounted on the *Blowfish* arms. Therefore when *Blowfish* is rotated there is movement of the optical fibers going from the LED box to the monitor detector. On the other hand there is no relative movement between the LED boxes and the *Blowfish* cells. This suggests that an improvement in the gain monitoring system could be achieved by mounting the monitor detector box somewhere on the *Blowfish* arms.

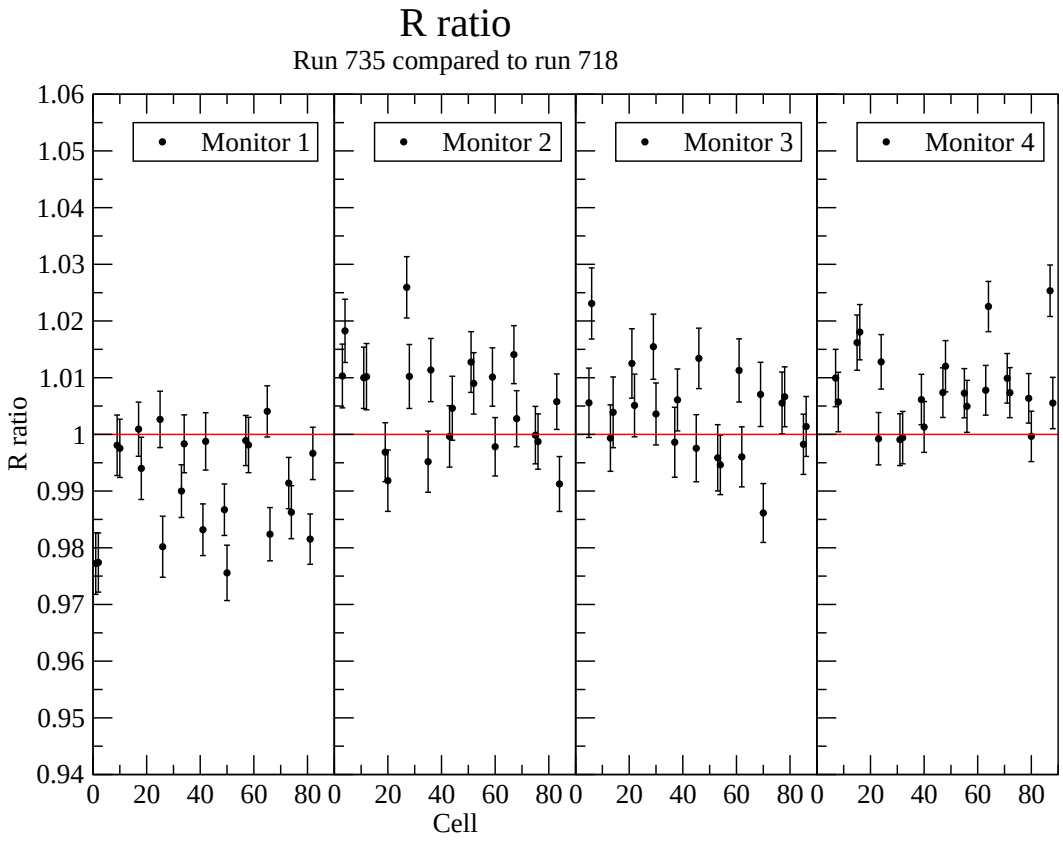

Figure 8: The value of R_i for a particular run divided by the value of R_i for an earlier run. The ratios are plotted for all cells and are subdivided according to the LED/Monitor to which the cell is linked.

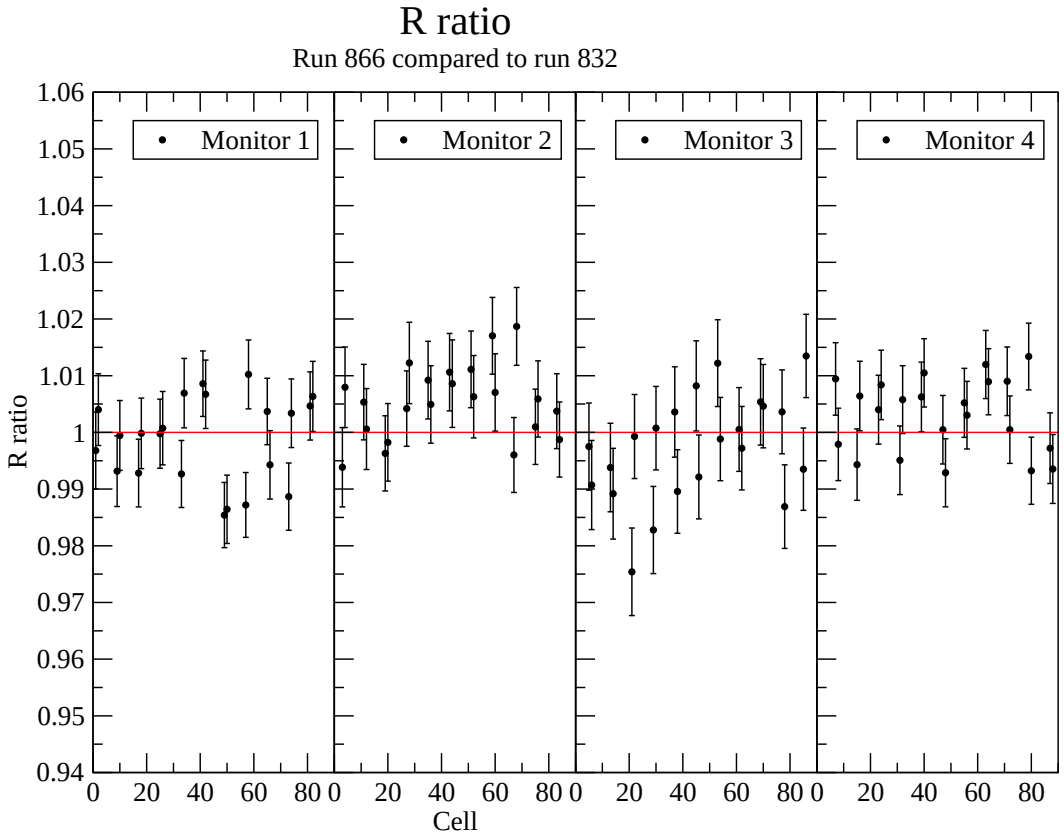

Figure 9: The value of R_i for a particular run divided by the value of R_i for an earlier run. The ratios are plotted for all cells and are subdivided according to the LED/Monitor to which the cell is linked.

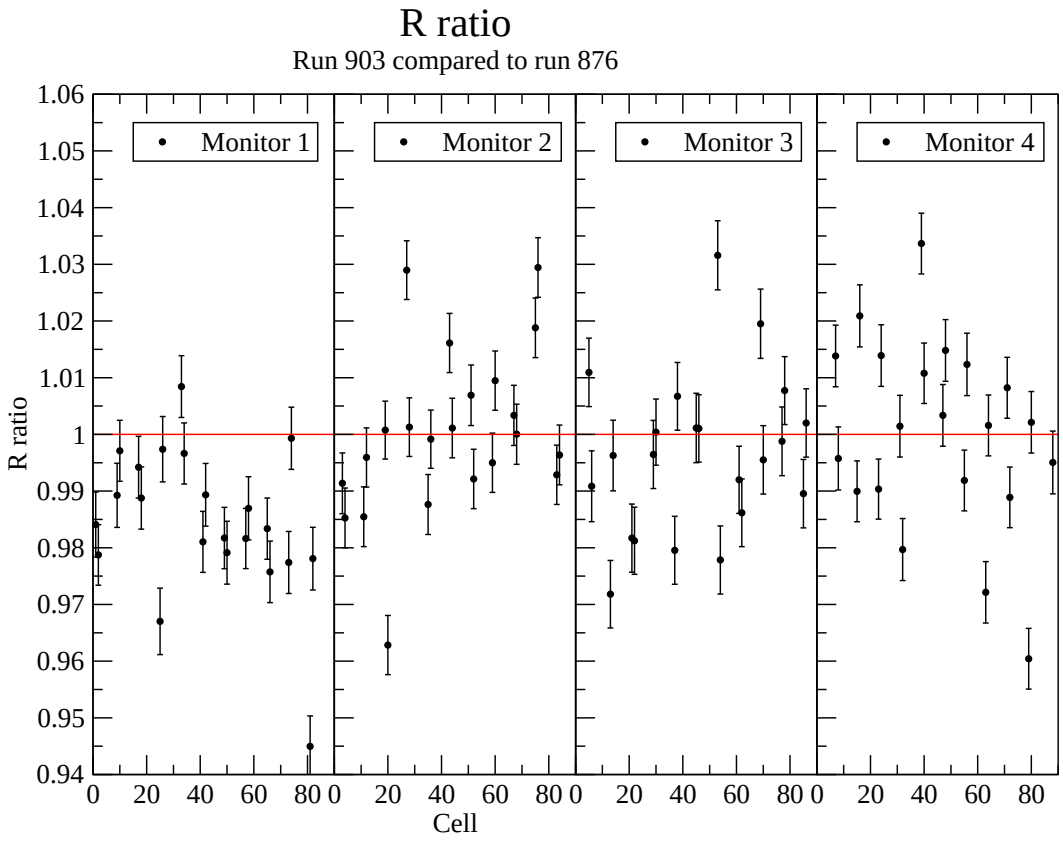

Figure 10: The value of R_i for a particular run divided by the value of R_i for an earlier run. The ratios are plotted for all cells and are subdivided according to the LED/Monitor to which the cell is linked.

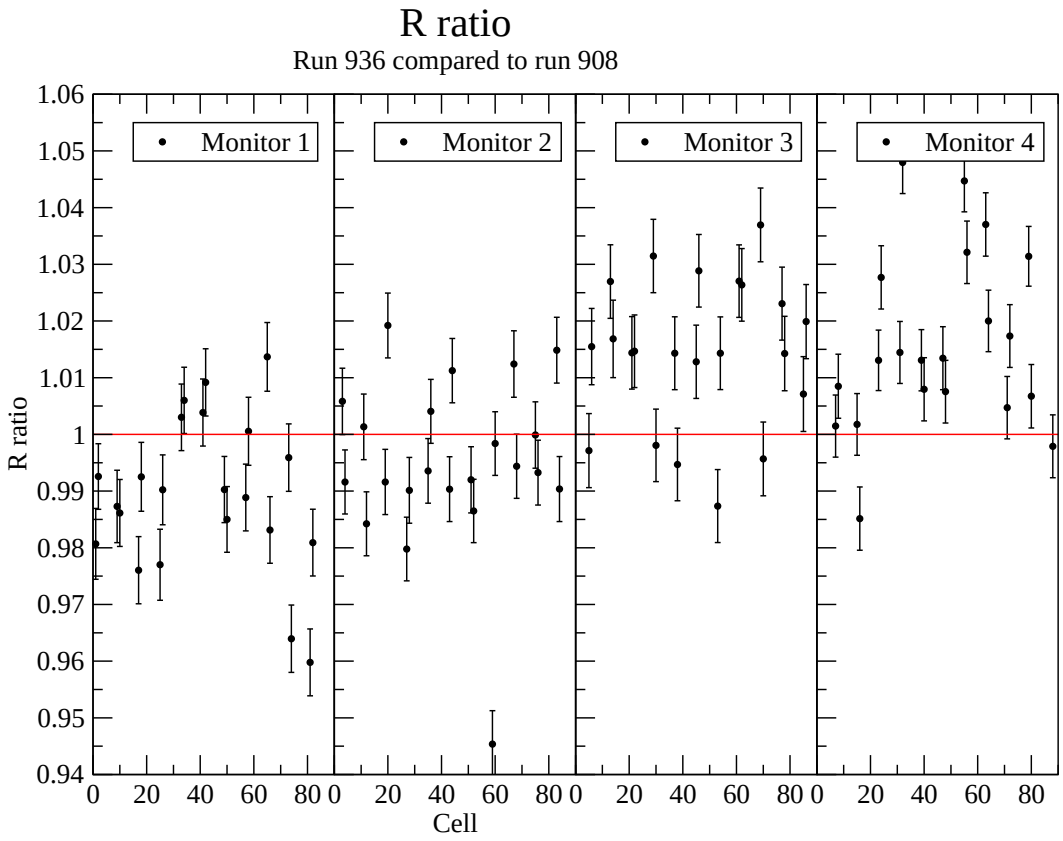

Figure 11: The value of R_i for a particular run divided by the value of R_i for an earlier run. The ratios are plotted for all cells and are subdivided according to the LED/Monitor to which the cell is linked.

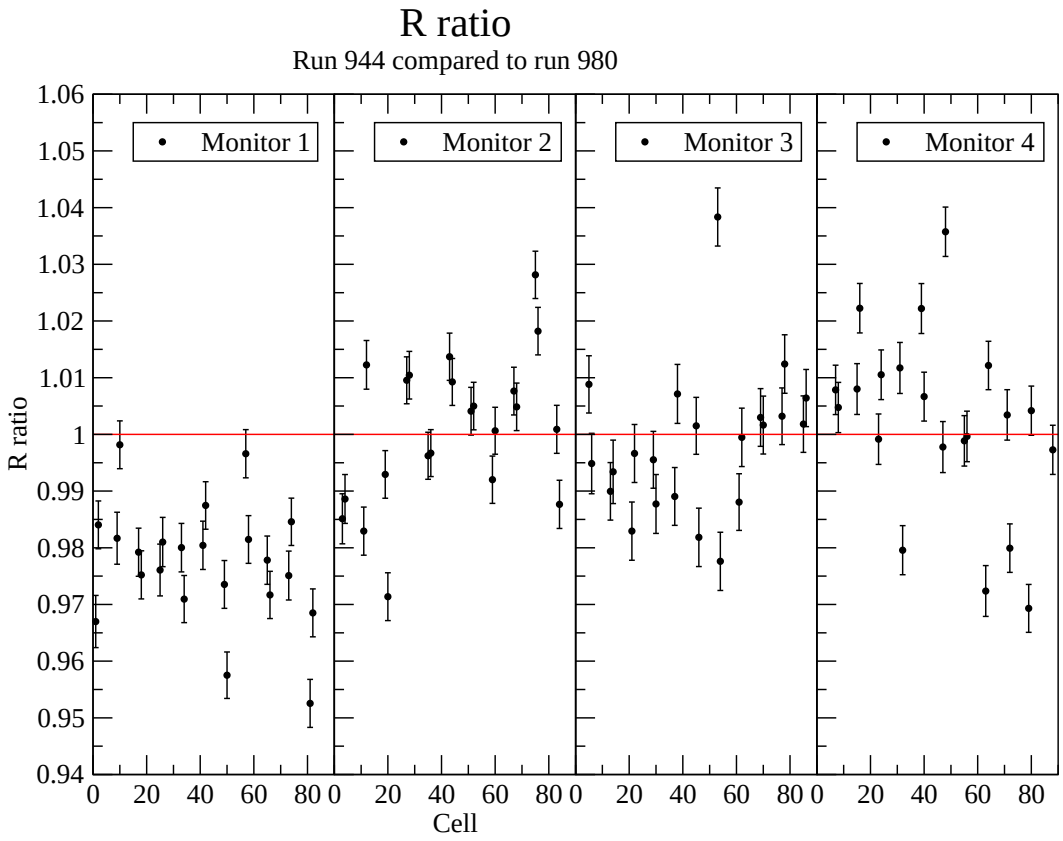

Figure 12: The value of R_i for a particular run divided by the value of R_i for an earlier run. The ratios are plotted for all cells and are subdivided according to the LED/Monitor to which the cell is linked.

3.3 Predicting Gains

We will now investigate how well equation 14 can determine the correct gain. We can check this by comparing the gain determined in a particular calibration run to that predicted by using the R_i values determined in an earlier calibration run. The results of this analysis are presented in figures 13-18. Two data sets are shown in these plots. First is the gain error that would result if no correction using the flasher data was made; i.e. the gain for the earlier run was simply used as the assumed gain for the present run. This percentage error is calculated using

$$\text{Gain Error} = \frac{(g_{early} - g_{present})}{g_{present}} \times 100\%$$

Second is the gain error using the gain predicted for the present run using the R_i values from the earlier run and the flasher information from the present run. This percentage error is calculated using

$$\text{Gain Error} = \frac{(g_{predicted} - g_{present})}{g_{present}} \times 100\%$$

It can be seen that the predicted gain is in general within a few percent of the correct gain. This is the case even when fairly large changes in gain have occurred; sometimes larger than 10%. This we feel is very satisfactory and is consistent with the measurements made by Bewer[5].

However, in some cases, systematic errors in the gain can be observed. For example in run 980, the predicted gains for cells associated with LED/Monitor 1 are systematically higher than the actual gain. These systematic errors are correlated with the systematic shifts in R_i values noted in the previous section. This is a further indication that the gain monitoring system might be improved by mounting the monitor box on the rotating portion of *Blowfish*.

The errors for the predicted gains shown in figures 13-18 are from statistical and curve fitting errors only. Because of the observed shifts in the R_i values an additional uncertainty in R_i (along with the statistical uncertainty) should be included in the calculation of the predicted gain.

However, before pursuing this further, we must take a look at some other aspects of gain determination.

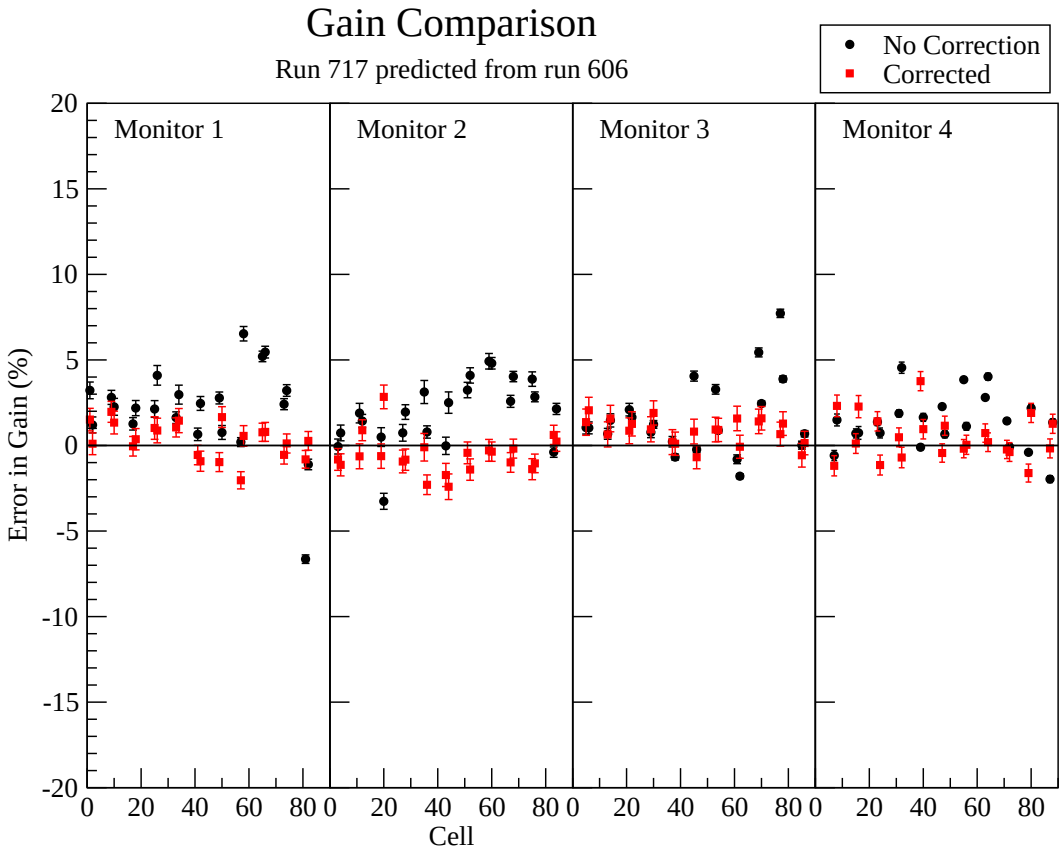

Figure 13: The percentage errors in the gains predicted for a run using the R_i values found from an earlier run are shown. Also shown are the percentage errors that would result if the gain from the earlier run was used instead of the predicted gain.

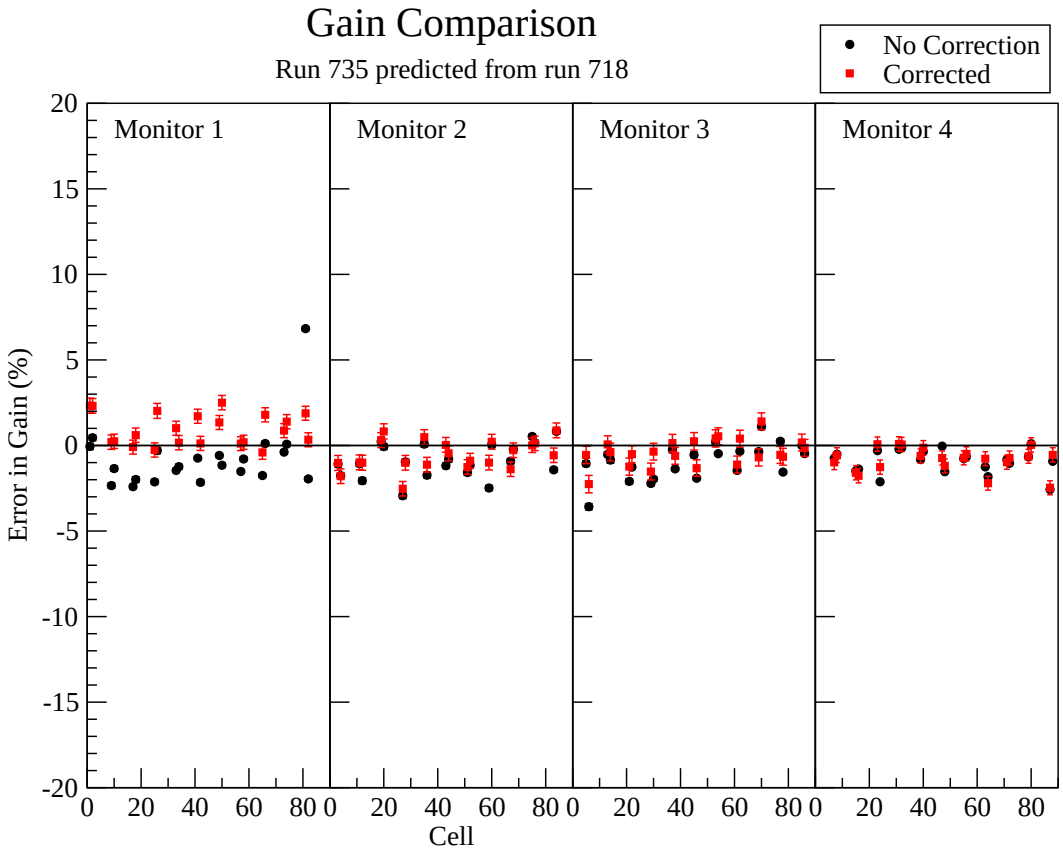

Figure 14: The percentage errors in the gains predicted for a run using the R_i values found from an earlier run are shown. Also shown are the percentage errors that would result if the gain from the earlier run was used instead of the predicted gain.

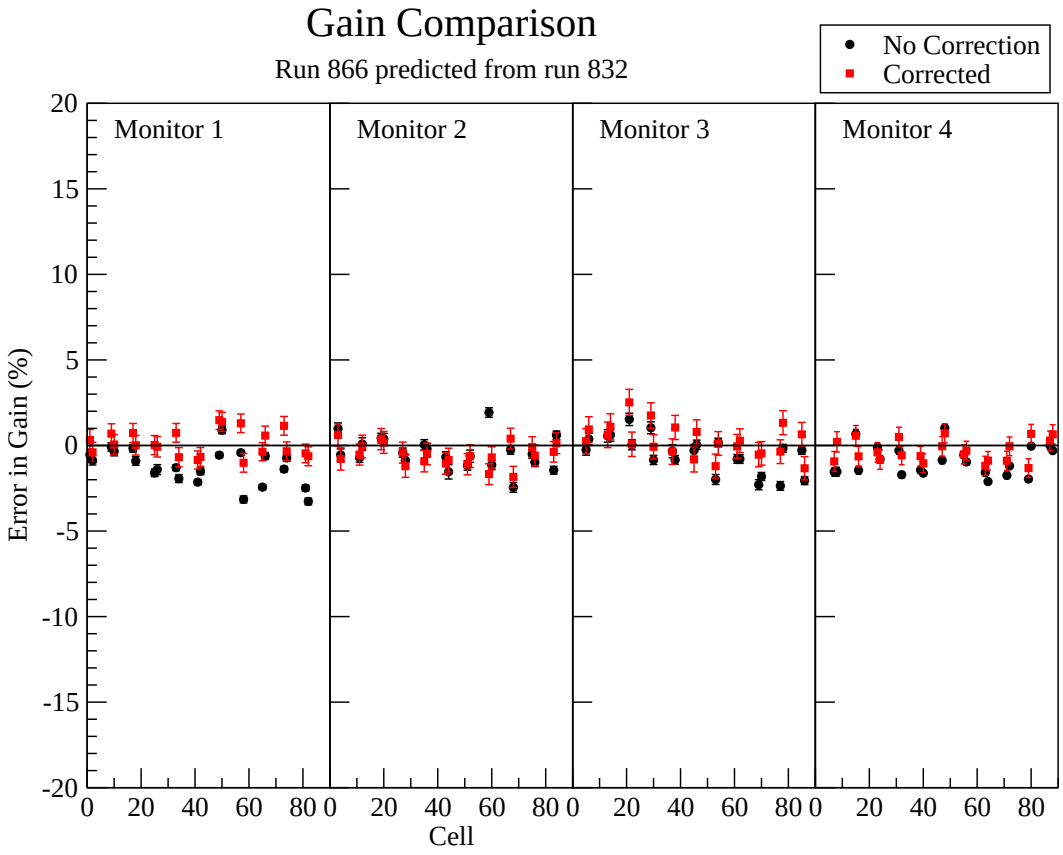

Figure 15: The percentage errors in the gains predicted for a run using the R_i values found from an earlier run are shown. Also shown are the percentage errors that would result if the gain from the earlier run was used instead of the predicted gain.

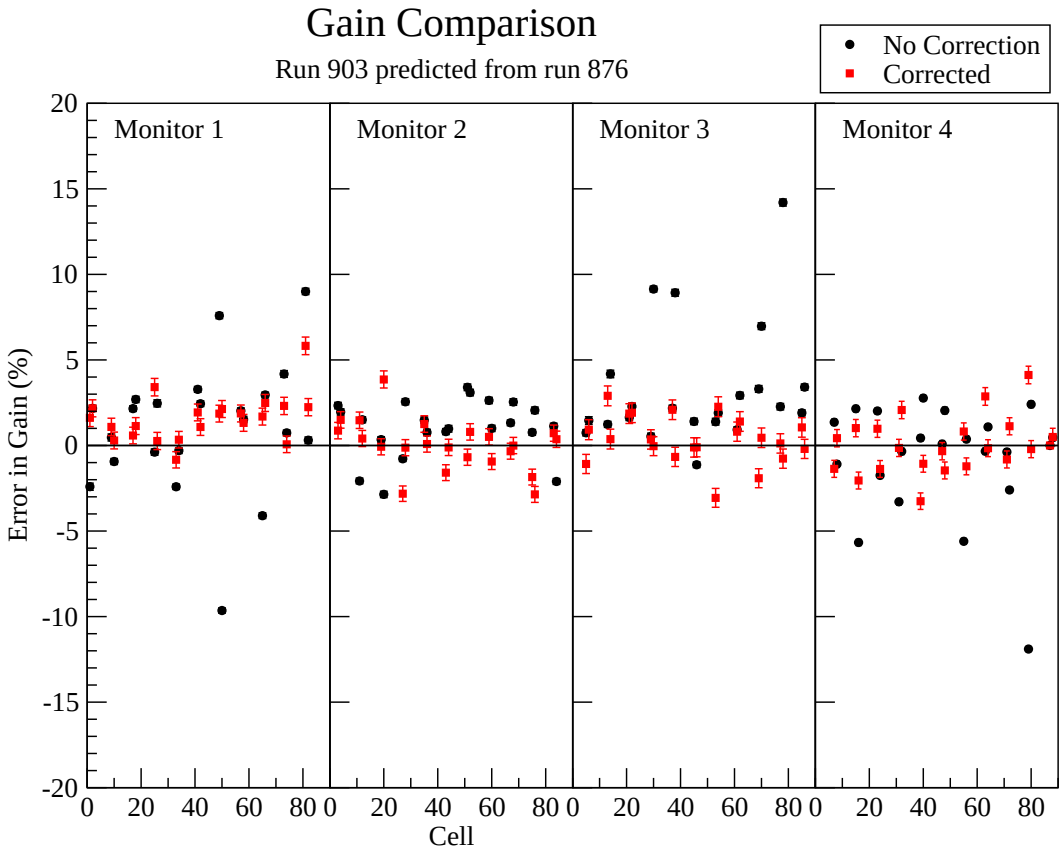

Figure 16: The percentage errors in the gains predicted for a run using the R_i values found from an earlier run are shown. Also shown are the percentage errors that would result if the gain from the earlier run was used instead of the predicted gain.

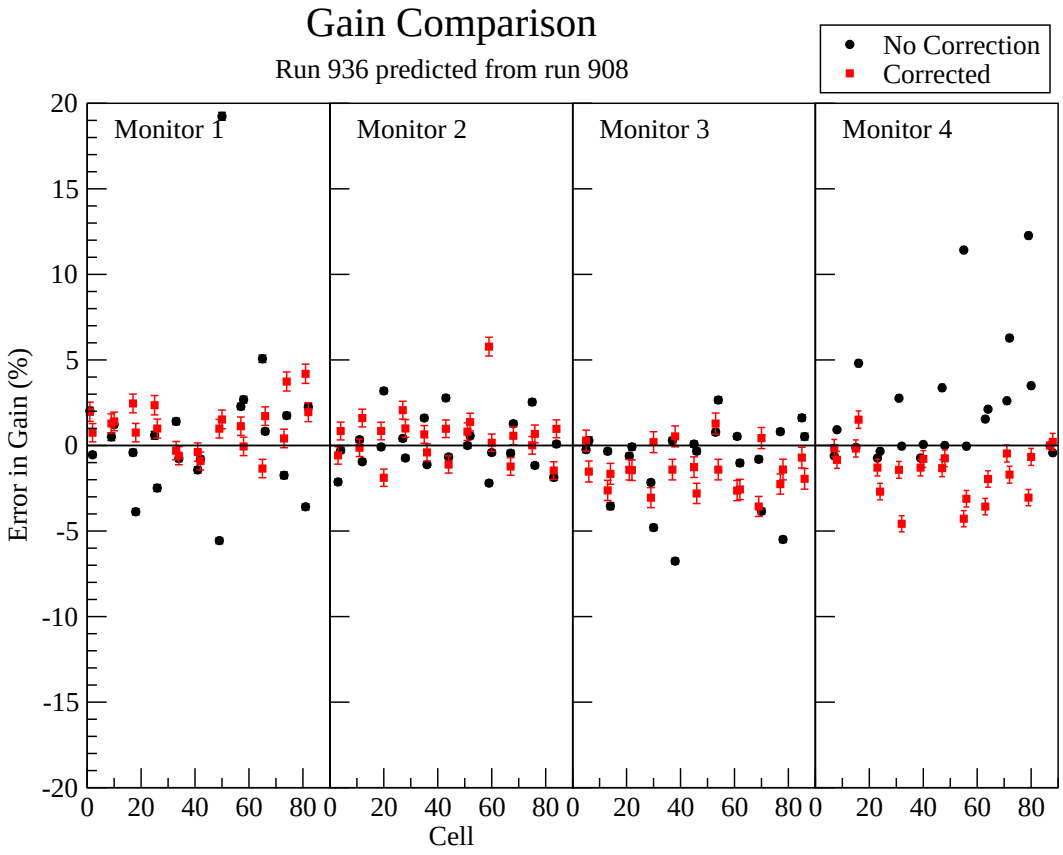

Figure 17: The percentage errors in the gains predicted for a run using the R_i values found from an earlier run are shown. Also shown are the percentage errors that would result if the gain from the earlier run was used instead of the predicted gain.

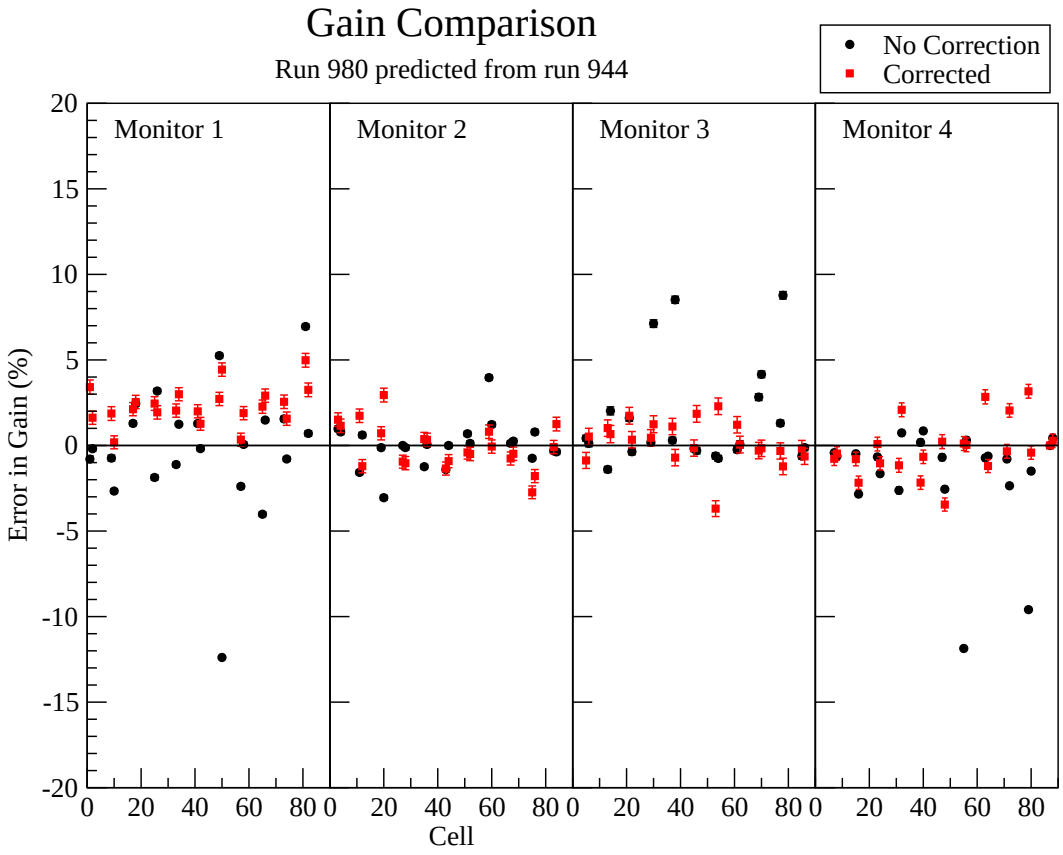

Figure 18: The percentage errors in the gains predicted for a run using the R_i values found from an earlier run are shown. Also shown are the percentage errors that would result if the gain from the earlier run was used instead of the predicted gain.

4 Gain Anomalies

All of the above looks fine as far as the gain monitoring system is concerned. However, some anomalies in the measured gains have been observed. Therefore, before proceeding further with establishing the gains for individual runs, we will first examine these anomalies.

4.1 Gains from Different Sources

At the end of the June/July 2008 run period four calibration runs were taken one after the other. Two using the Thorium Source and two using the AmBe source. The gains determined from these four runs should be the same since no changes were made between them and any gain drifts over this short time period should be minimal. Figure 19 compares the gains from these four runs. The gains for runs 397 and 398 were determined using the 2.614 MeV gamma ray from the Thorium source and the gains from runs 399 and 400 were determined using the 4.430 MeV gamma ray from the AmBe source. It can bee seen that the gains for runs 397 and 398 agree well but the gains determined using the AmBe source are significantly lower.

It is possible to make a similar comparison for the September/October 2008 running period. No data was taken using the Thorium source however the room background contains a strong Thorium peak. Therefore gains using the 2.614 MeV gamma ray from Thorium were obtained from run 907. This is compared to the gain determined from run 908 using the AmBe 4.430 MeV gamma ray in figure 20. We see a similar shift in gain for these runs however the magnitude of the shift is significantly smaller.

This observation draws into question the assumptions behind the gain determination procedure.

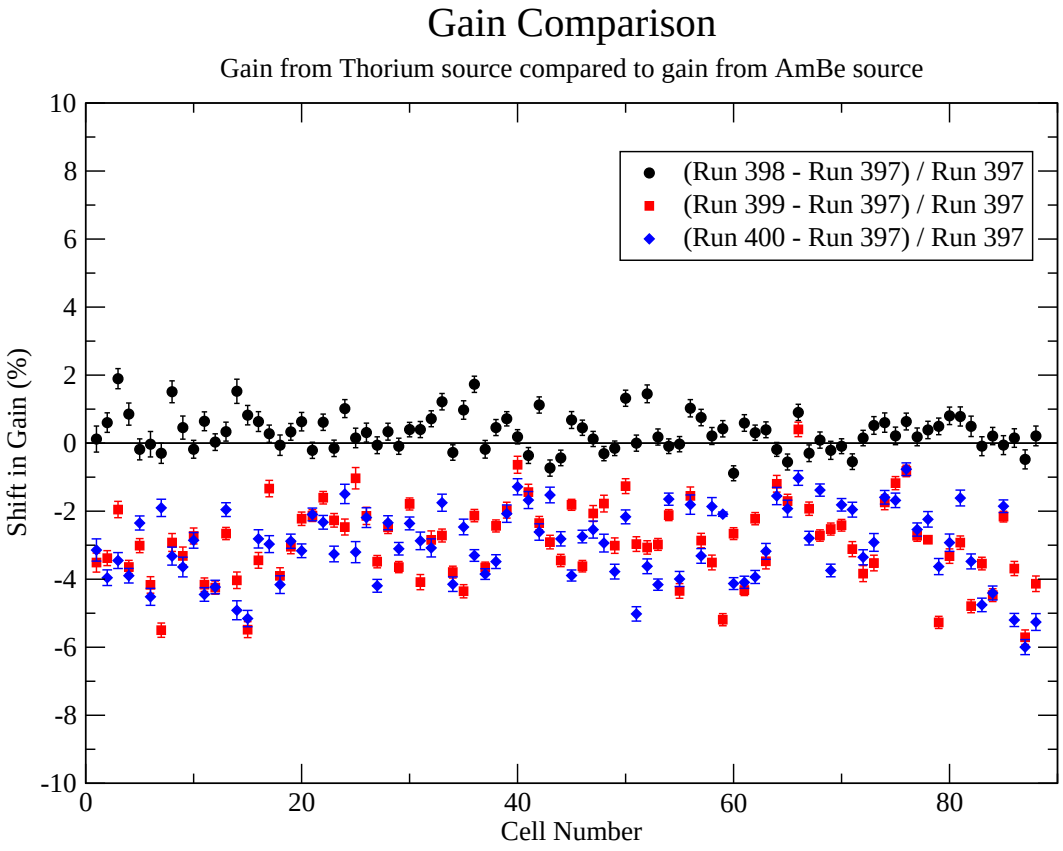

Figure 19: The gains from four consecutive runs from the June/July run period are compared. The gains for runs 397 and 398 were determined using the 2.614 MeV gamma ray from the Thorium source and the gains from runs 399 and 400 were determined using the 4.430 MeV gamma ray from the AmBe source.

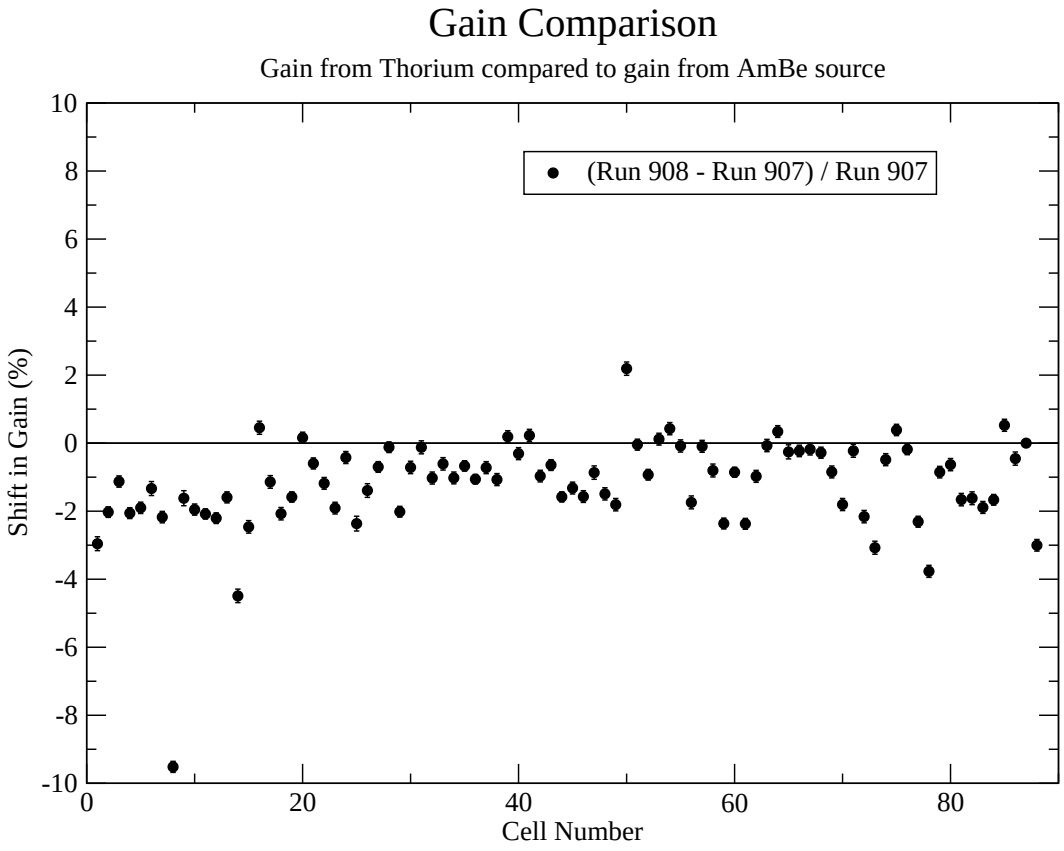

Figure 20: The gains from two runs in the September/October run period are compared. The gains for run 907 was determined using the 2.614 MeV gamma ray from the Thorium in the room background and the gain from run 908 was determined using the 4.430 MeV gamma ray from the AmBe source.

4.2 Pulse Integration Time Effects

Further evidence for an error in the gains was noted by Blackston [6] and confirmed by Wurtz. Both have noted a need to increase the measured neutron light output energy scale in order to get good agreement between measured light output spectra and those predicted by a GEANT4 simulation. This has been attributed to the charge integration time for the ADC being too short. The charge integration time is set by the gate applied to the VME ADCs. Because neutron pulses are in general longer than gamma ray pulses it was suggested that the tail end of the pulse is being clipped of. Thus the effective gain for neutron pulses is smaller than for gamma rays.

Some evidence that contribute to understanding this comes from a test we performed during the September/October running period. This test was designed to check if a long cable inserted between a neutron cell and the ADC had any detrimental effect on the quality of pulse shape discrimination (PSD). Using an AmBe source light output spectra were recorded with and without the long cable present. The long cable has the effect of increasing the pulse time constants (rise and fall times) for both gamma ray and neutron pulses. The result was that no loss in PSD quality was observed. However it is the effect of the long cable on pulses themselves which is of interest here.

If the long gate was sufficiently long to integrate the full pulse for both the long and short cable situations, no change in gain (after proper pedestal subtraction) should be observed. If the long gate is too short and tail end of the stretched long-cable pulse was being clipped we would expect a decrease in ADC value. What we observe is shown in figure 21.

First we note that the effective threshold has increased when the long cable is used. This is to be expected since the long-cable stretched pulse has a lower pulse height and the discriminator acts at a constant fraction of pulse height.

The long-gated ADC pulse height has *increased* rather than decreased as would be expected if the tail of the pulse was being clipped. The short-gated ADC pulse height has decreased as expected since more of the long-cable stretched pulse will be beyond the end of the short gate. These observations suggest that if clipping is occurring, it is at the *beginning* of the integration time, i.e. the ADC gates do not start soon enough. This would explain the increased pulse height for the long-gated ADC since less of the long-cable stretched pulse will be missed before the integration time starts.

The above argument is based on pulse height information for gamma rays only. Although the possibility of the tail of neutron pulses being clipped is not ruled out, it would appear to be unlikely because we have scope images of neutron pulses which appear to fall within the 200 ns ADC gate length. The hypothesis of pulse clipping certainly needs to be investigated further.

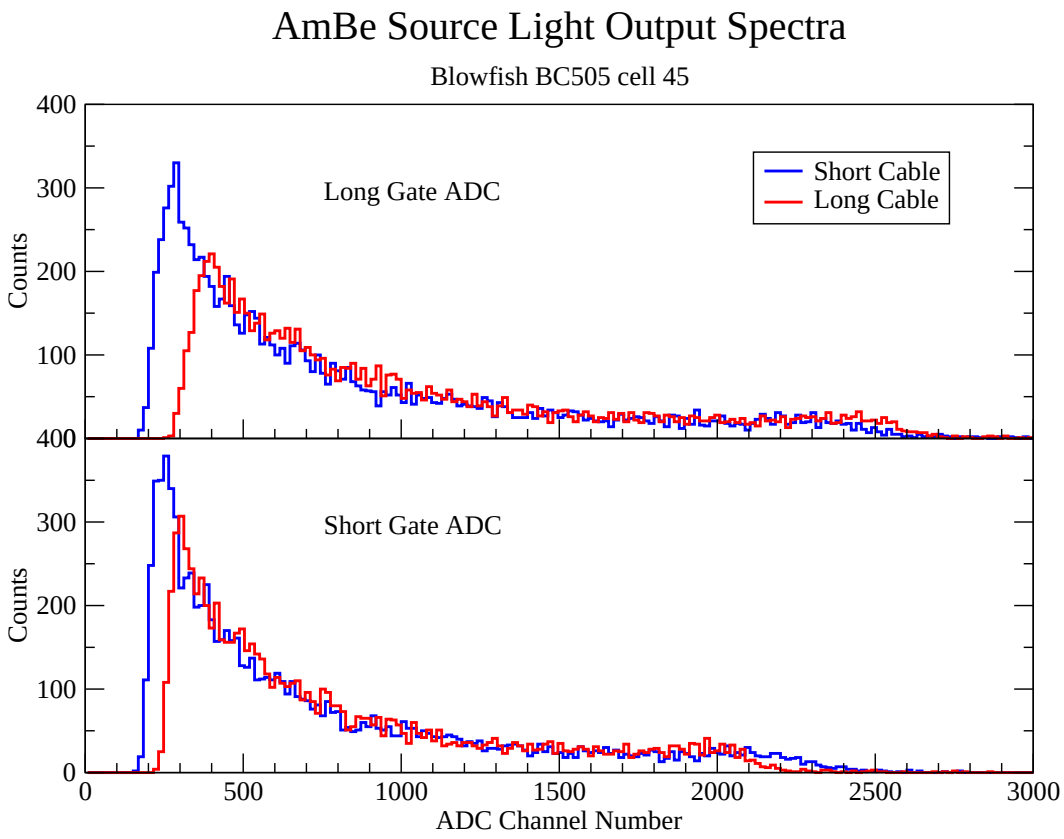

Figure 21: The effect of changing cable lengths on the light output spectra from an AmBe source.

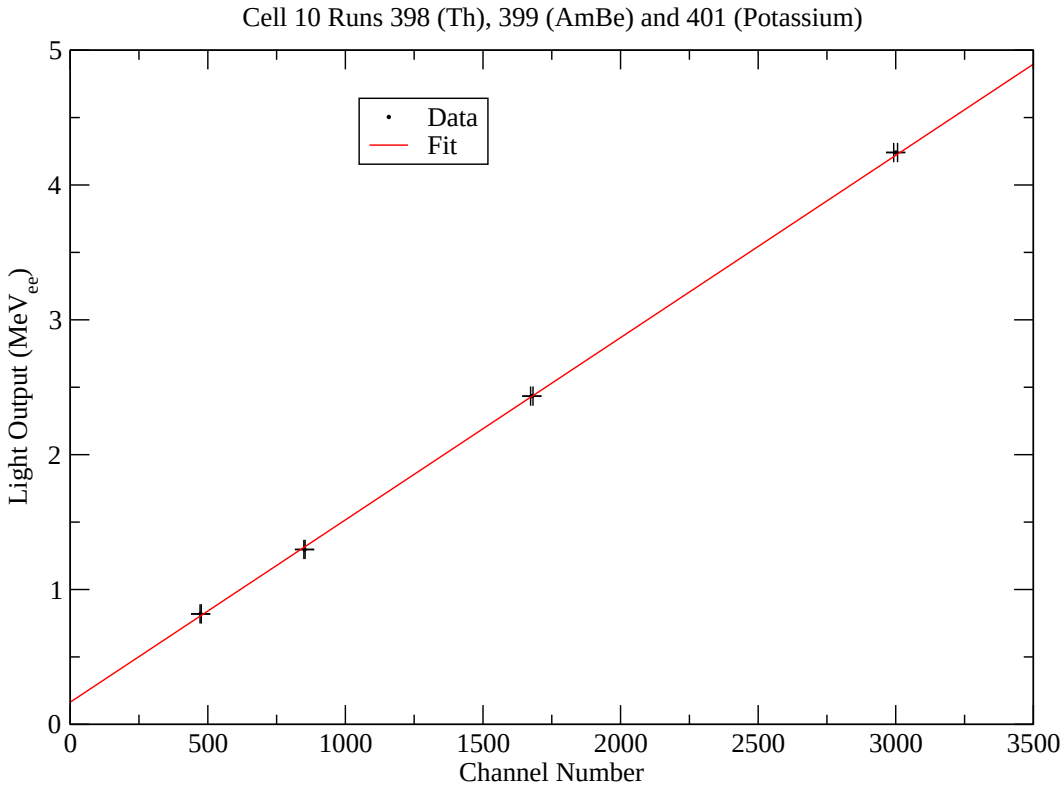

Figure 22: Energy verses channel number obtained from four data points: the 0.968 MeV and 2.614 MeV Thorium gamma rays from run 398, the 4.430 MeV AmBe gamma ray from run 399, and the 1.461 MeV Potassium-40 gamma ray from the room background run 401. The line is the best fit straight line.

4.3 Gain Linearity and Offsets

The gain inconsistencies noted in section 4.1 suggest the possibility of a nonlinear gain function. Further, the possibility of pulse clipping noted in section 4.2 suggests a non-zero offset in the gain function. To investigate this we attempt to find multiple calibration points for some specific situations.

As noted before, at the end of the June/July running period several calibration runs we recorded using both the Thorium and the AmBe sources. I addition a long room background run was taken. The Thorium source contains two prominent gamma rays at 0.968 MeV and 2.614 MeV. The AmBe source has the 4.430 MeV gamma ray. The room background contains, in addition to the 2.614 MeV Thorium gamma ray, a rather prominent 1.461 MeV gamma ray from Potassium-40. Fitting to the Compton edges for these four gamma rays in runs 398, 399 and 401 gives a calibration curve. This is displaced for one cell (cell 10) in figure 22.

The four data points are fitted excellently by a straight line. The non-zero energy offset explains why, in section 4.1 we found different gains using different sources if we assume a zero offset.

We get a similar straight line fit for all other *Blowfish* cells. Figure 23 shows the fitted

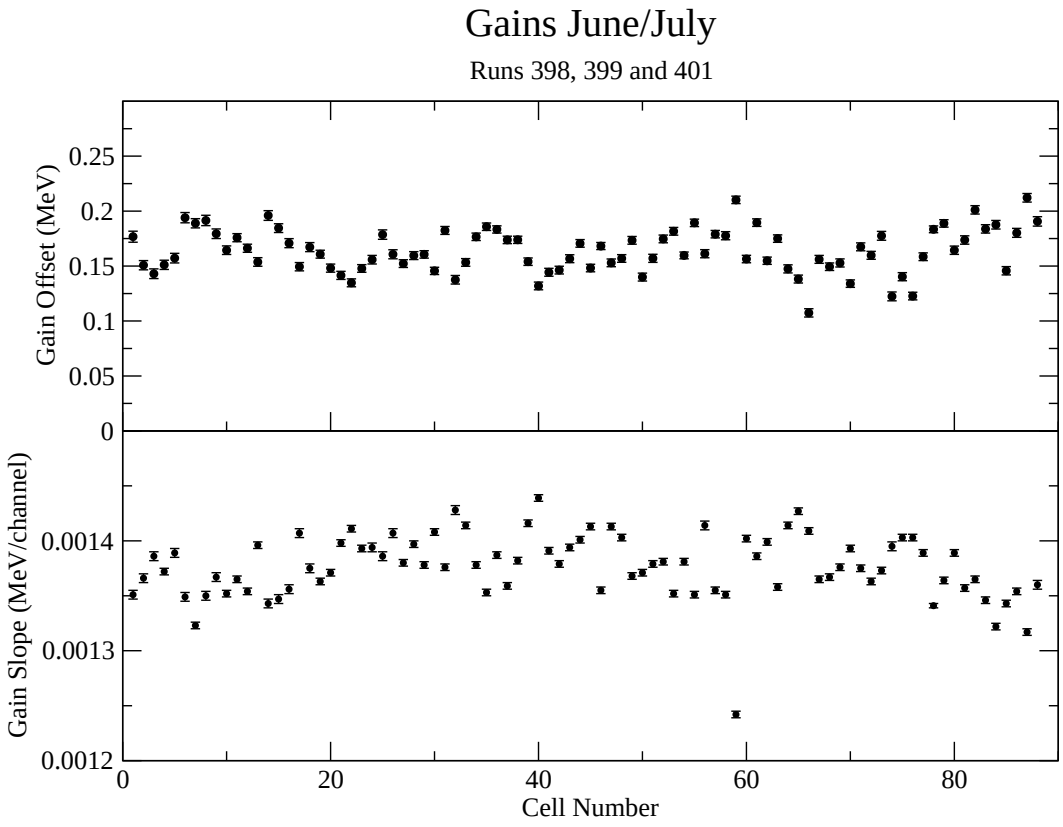

Figure 23: The fitted slope and offset for all cells derived from runs 398, 399 and 401 in the June/July running period.

offset and slope of the gain curve for all cells. Note that the offset is about the same for all cells.

We are able to find a similar gain curve for the September/October running period. Here we use the 4.430 MeV AmBe gamma ray from run 908 and from the background run 907 we fit to the Thorium 2.614 MeV gamma ray and to the Potassium-40 1.461 MeV gamma ray. these three data point are plotted for one cell in figure 24. Again an excellent straight line fit is found. In this case however the energy offset is much smaller than for the June/July running period.

Figure 25 shows the fitted offset and slope of the gain curve for all cells. Once again we note that the energy offset is approximately the same for all cells.

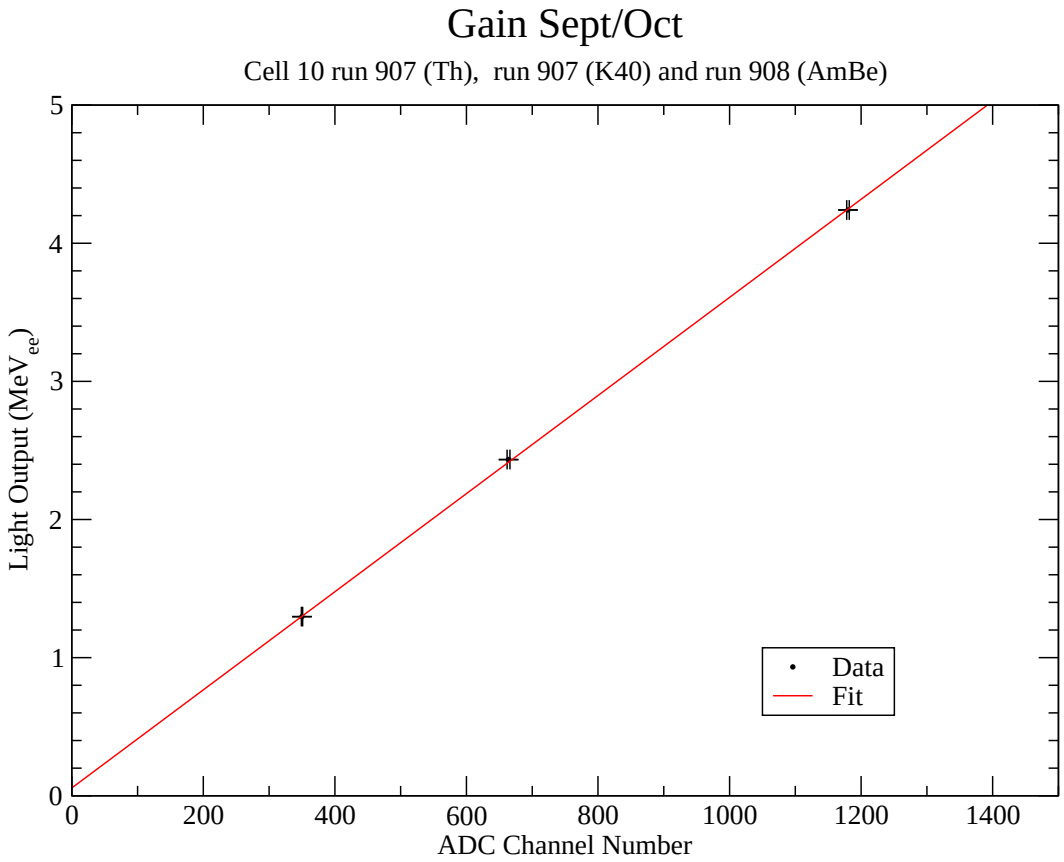

Figure 24: Energy verses channel number obtained from three data points: the 4.430 MeV AmBe gamma ray from run 908 along with the 2.614 MeV Thorium gamma ray and the 1.461 MeV Potassium-40 gamma ray from the room background run 907. The line is the best fit straight line.

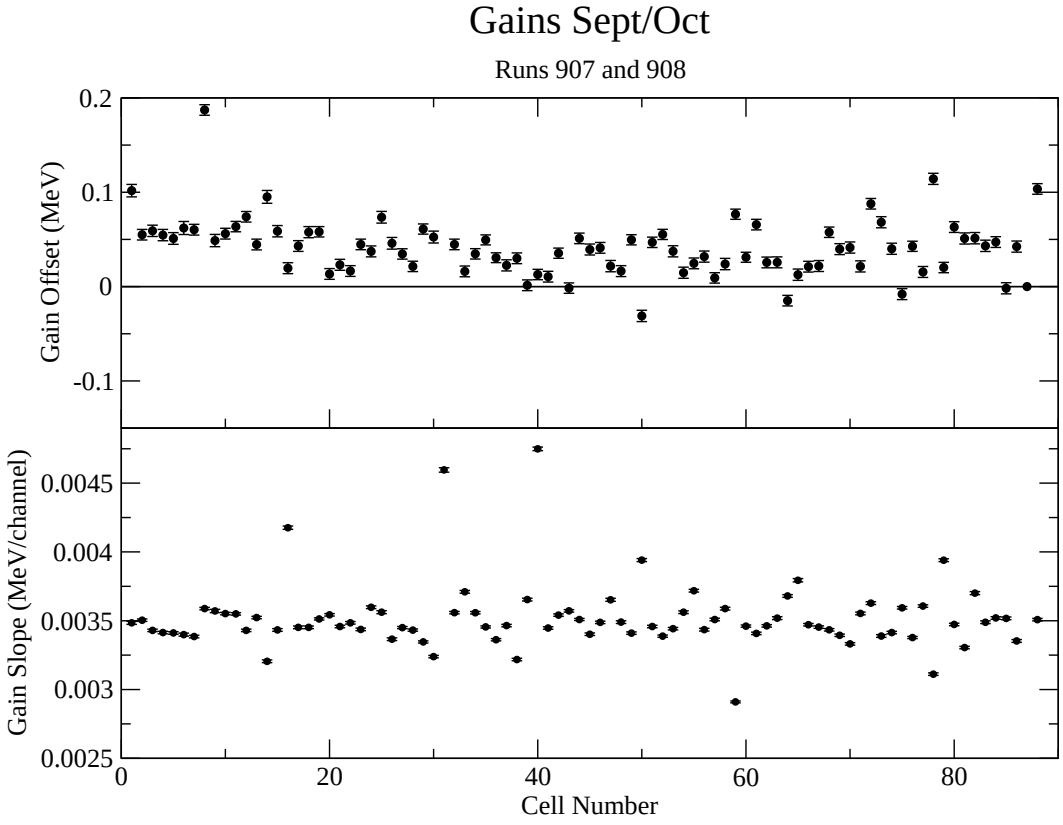

Figure 25: The fitted slope and offset for all cells derived from runs 907 and 908 in the September/October running period.

4.4 The Origin of the Energy Offset

The non-zero energy offset apparent in both gain curves implies that we are missing some of the energy in each pulse. This might be consistent with clipping of the pulse due to a too short integration time not covering the whole pulse.

The fact that the energy offset is much smaller for the September/October running period compared to the June/July running period may be significant. The data acquisition electronics was entirely rebuilt before the September/October running period and the ADC gate timings were reset carefully. Perhaps this reduced the integration time clipping effect. The fact that some offset remains for the September/October run may indicate that the time between the start of the ADC gate and the time the ADC actually starts integrating is longer than stated in the manual. Another relevant difference between the September/October run period and the June/July run period is that the higher energy September/October runs used much lower Photomultiplier gains (and therefore lower high voltages).

The details of how clipping might result in the observed gain curves is not clear. One possible explanation has to with TDC walk. Although constant fraction discriminators are used a small residual time shift as a function of pulse height is observed.

Suppose that the shape of a gamma ray pulse can be represented by a function $f(t)$ where

$$\int_0^\infty f(t)dt = 1$$

and $f(0) = 0$ and $f(\infty) = 0$. If the light output for a particular gamma ray is L then the pulse may be represented by $p(t) = Lf(t)$. If the full pulse is integrated then

$$L = \int_0^\infty p(t)dt \tag{15}$$

as expected. If clipping occurs at a constant time t_s after the start of the pulse, then the measured output M will be

$$M = \int_{t_s}^\infty p(t)dt = L\int_{t_s}^\infty f(t)dt. \tag{16}$$

Therefore M is still proportional to L which agrees with the observed linear gain curves but is at variance with the observation of an energy offset.

Suppose that the TDC introduces a time walk which is minimal for large pulses but larger for small pulses. This time walk will shift the integration start time by an amount $t_s \to t_s + w/L$, where w is a constant. This is equivalent to shifting the whole pulse by this time shift; i.e.

$$f(t) \to f(t - w/L) \approx f(t) - \frac{w}{L}\frac{df(t)}{dt}$$

for small walks. The measured output then becomes

$$\begin{aligned} M &= L\int_{t_s}^{\infty} f(t - w/L)dt \\ &\approx L\int_{t_s}^{\infty} \left(f(t) - \frac{w}{L}\frac{df(t)}{dt} \right) dt \\ &= L\int_{t_s}^{\infty} f(t)dt - wf(t)|_{t_s}^{\infty} \\ &= L\int_{t_s}^{\infty} f(t)dt - w\left[f(\infty) - f(t_s)\right] \\ &= L\int_{t_s}^{\infty} f(t)dt + wf(t_s)\ . \end{aligned} \tag{17}$$

We see that the second part of equation 17 is a piece of the observed output that is independent of L and is therefore a possible explanation for the energy offset observed in figures 22 and 24.

Ward Wurtz has made an estimate of w [7]. The time difference between the accelerator bunch trigger and a Compton scattered gamma ray reaching a cell is excellently fitted by a function of the form w/L. This yields a value of $w = 67 \pm 2$ ns $\cdot$ keV$_{ee}$.

We can use this to make an estimate of the expected energy offset due to the time walk effect. We assume that the pulse can be described by a function

$$f(t) = \frac{1}{(t_r - t_f)}\left(e^{-t/t_r} - e^{-t/t_f}\right)$$

which is normalized so that

$$\int_0^{\infty} f(t)dt = +1.$$

The maximum energy offset will be when t_s is such that $f(t_s)$ has a maximum value. The maximum value of $f(t)$ is at a time

$$t_{max} = \frac{1}{1/t_r - 1/t_s}\ln\left(\frac{t_f}{t_r}\right)\ .$$

We assume values for the rise time and fall time of about t_r =1 ns and t_f =20 ns. For these values $f(t_{max}) = 0.043$ ns^{-1} which yields an energy offset of 3 keV. Changing t_r and t_f over a wide range of reasonable values we find that the maximum energy offset is always less than about 6 keV.

Therefore it appears that time walk cannot completely account for the large energy offsets observed in the gain curves (figures 22 and 24).

Clearly there is an additional effect that we have not taken into account. Perhaps the explanation for the energy offset has something to do with the operation of the VME ADC that we do not understand. For example the ADC may be imposing an additional negative pedestal when the input is non-zero at the time the ADC starts integrating. Or perhaps there is something about the photomultipliers and/or bases that is not understood. This is perhaps suggested by the fact that the offset is smaller when lower PMT voltages are used.

We admit that the above are speculations and a much more detailed experimental study of these effects is clearly needed. This would involve checking the effect on the gain curves, as determined using multiple sources, while things such as the ADC gate timing and widths are adjusted and PMT voltages are changed.

5 Light Output

A full understanding of the *Blowfish* BC-505 cell gains is necessary if the detector efficiency is to be calculated accurately. It is therefore important to be able to match the observed light output spectra to the GEANT4 simulation. It was noted in section 4.2 that Blackston[6] and Wurtz[7] found that the measured neutron light output spectra have end-points which are lower than that predicted by the GEANT4 simulation.

5.1 Light Output Spectra for Deuteron Photo-disintegration

To investigate this further we look for a situation where the neutron energy is known. We use the deuteron photo-neutron data taken during the September/October 2008 running period. Data was taken using a D_2O target at a photon energy of 20 MeV. From kinematics it is possible to calculate the neutron energy emerging at each angle with respect to the beam axis and arriving at a particular cell. We choose cells at 90° to the beam axis.

The neutron energy is calculated from time of flight. TDC time offsets are found using the Compton scattered gamma rays arriving at each cell. The time per channel for each TDC channel was found by inserting a cable of known time length into the TDC start signal line and observing the change in the position of the self-timing peak for each channel. The TDC calibration factors found in this way are plotted in figure 26.

A fairly large pulse height cut (of about 1 MeV_{ee}) was applied so that the PSD cut included almost no photons. Then for neutrons passing a PSD cut the neutron energy was calculated from the time-of-flight. The difference between the calculated neutron energy and the neutron energy expected from kinematics is shown for a few cells at 90° in figure 27. A clear peak at zero is visible. The peak at about −5 MeV is due to Oxygen.

It was noted that this energy difference peaked at about −0.2 MeV for many cells. This was corrected by reducing the flight time by 0.1 ns. There may be some justification for this. If the rise time of a neutron pulse is a bit longer than the rise time of a gamma pulse from the BC-505 cell then the flight time for a neutron is a bit shorter than that indicated by the discriminator stop time. However, it should be noted that such a small correction could also be made by adjusting the flight distance or adjusting the TDC calibration factor.

For neutrons in the energy difference peak the light output is plotted. (Neutrons within ±3 MeV of zero energy difference were included.) The same was done for the simulation. Only events with cell multiplicities of 1 are included in both cases. The results for three cells are shown in figures 28, 29 and 30.

It can be seen that measured light output does not agree well with the simulation result. The endpoint of the measured light output spectrum is clearly too low compared to the simulation. The cell gains used for the light output calculation are derived using the procedure outlined in section 2. In this case the gains for run 702 were calculated from the flasher data and the R_i values derived from the calibration run 717. The error introduced by ignoring a possible energy offset in the calibration curve is nowhere near enough to account for the observed energy error seen in figures 28, 29 and 30. (The energy offsets in figure 24 are less than 0.1 MeV.) Indeed the endpoint energy is very close to the energy of our calibration point using the AmBe source, so any gain error should be minimal at this energy.

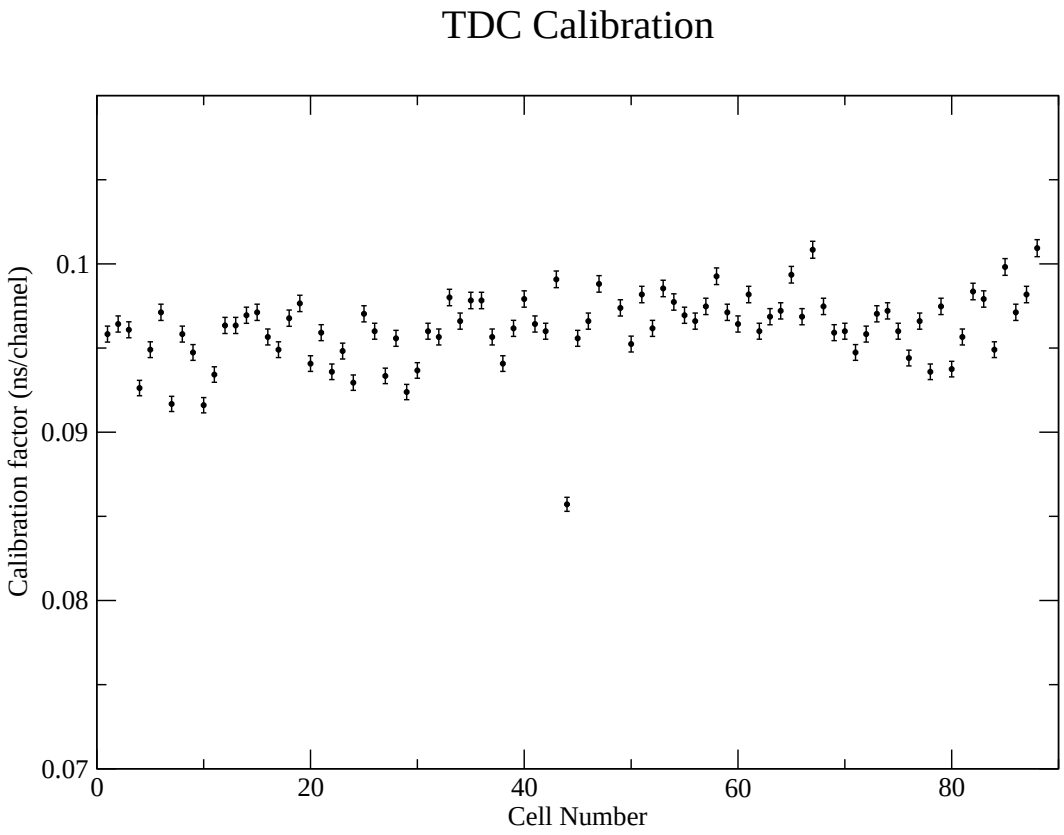

Figure 26: The TDC time per channel calibration for each cell determined from runs 515 and 516 when a cable of known time length was inserted into the TDC start signal. Note that the value for cell 44 is known to be in error from the analysis of deuteron photo-neutron data.

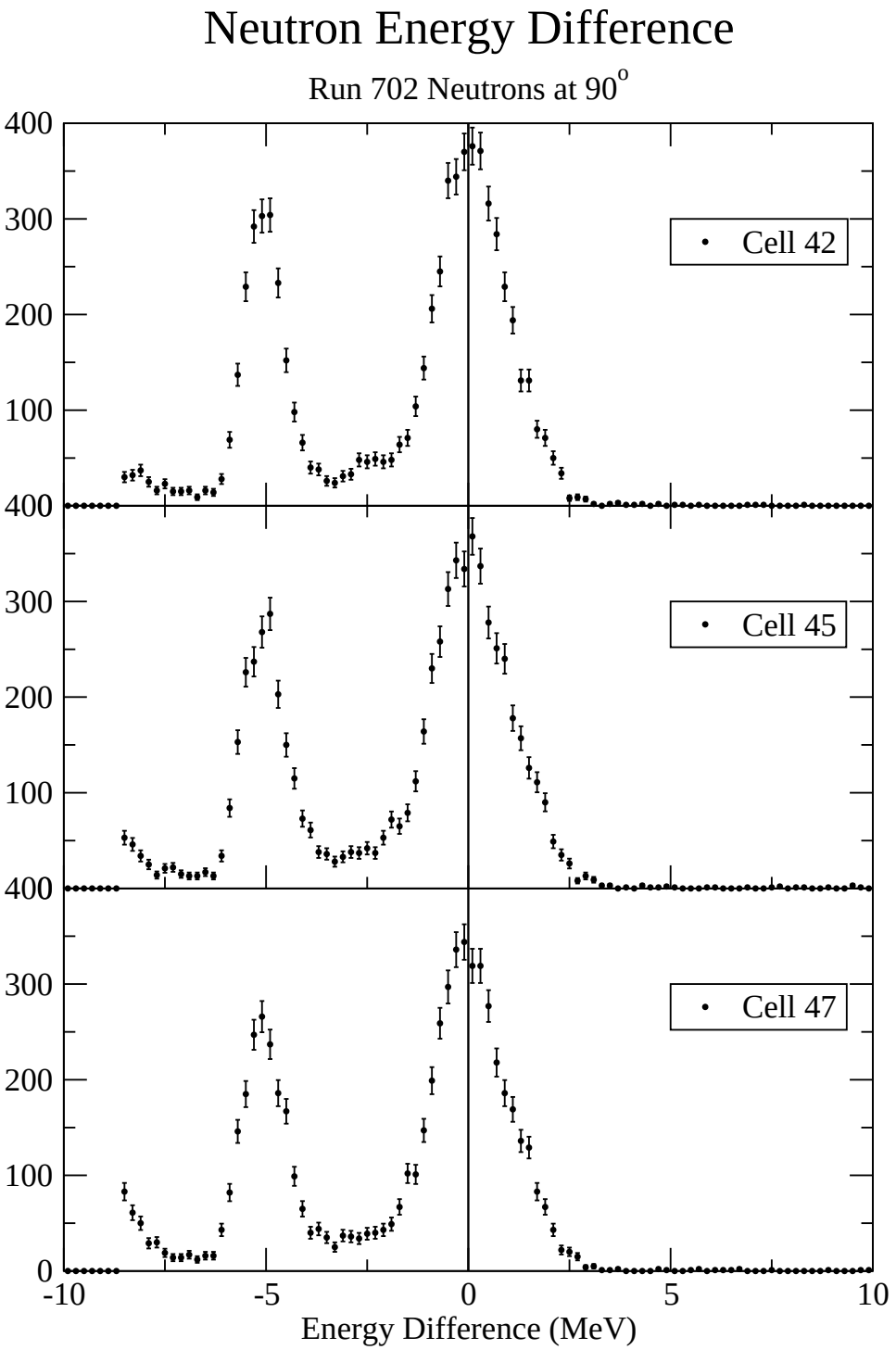

Figure 27: The difference between the neutron energy calculated from time-of-flight and the energy expected from deuteron photo-neutron kinematics is plotted for a few cells.

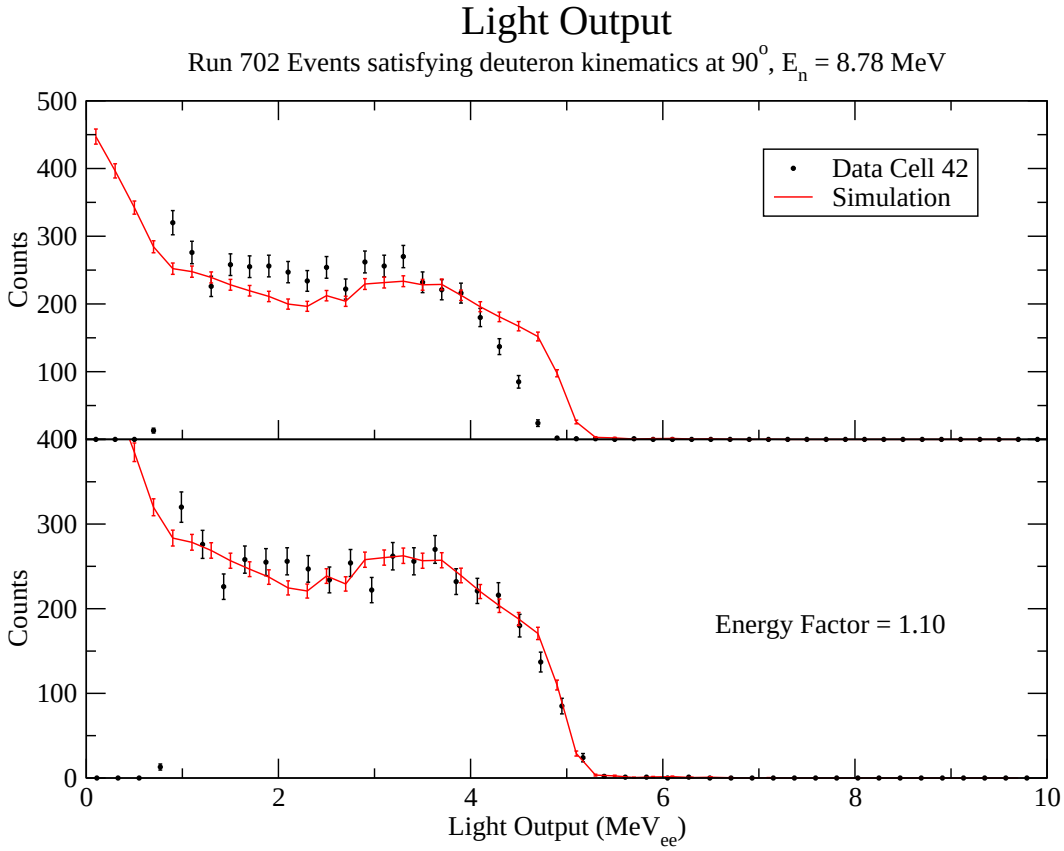

Figure 28: The light output for a cell at 90° for neutrons satisfying deuteron kinematics (i.e. with a neutron energy of 8.78 MeV) is plotted along with the simulated light output in the top graph. The lower graph shows the comparison when the light output energy scale has been multiplied by the energy factor noted.

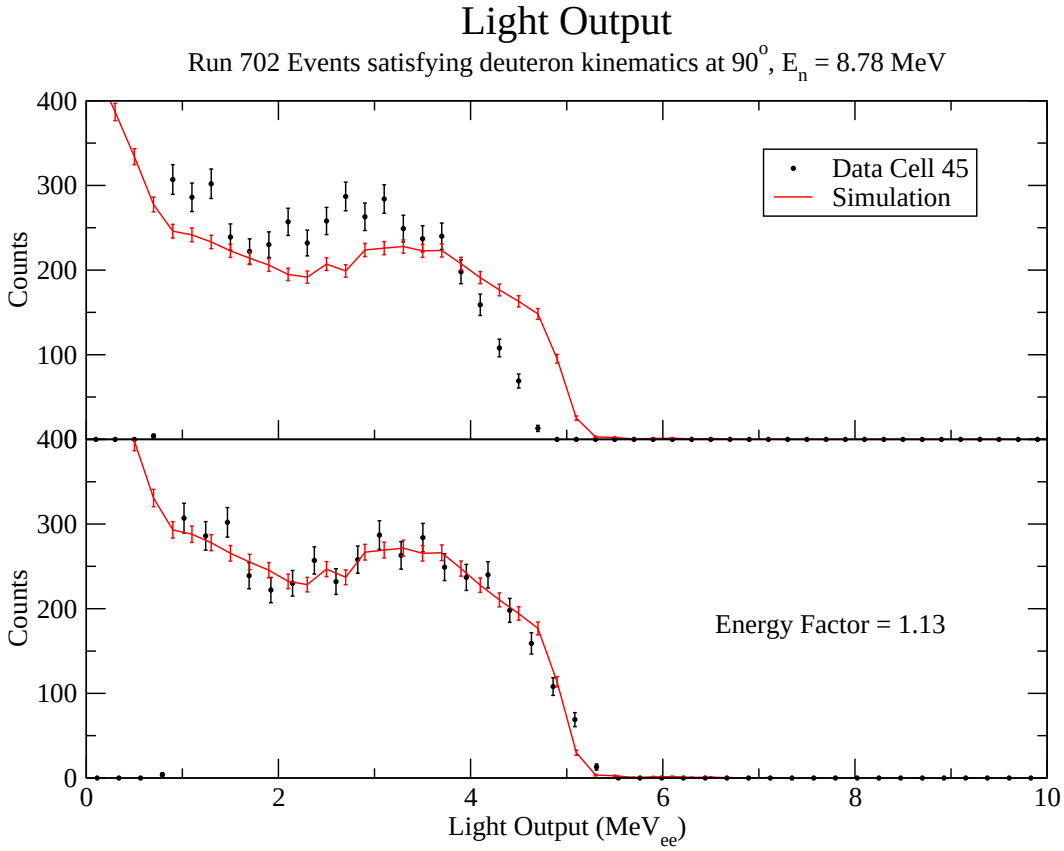

Figure 29: The light output for a cell at 90° for neutrons satisfying deuteron kinematics (i.e. with a neutron energy of 8.78 MeV) is plotted along with the simulated light output in the top graph. The lower graph shows the comparison when the light output energy scale has been multiplied by the energy factor noted.

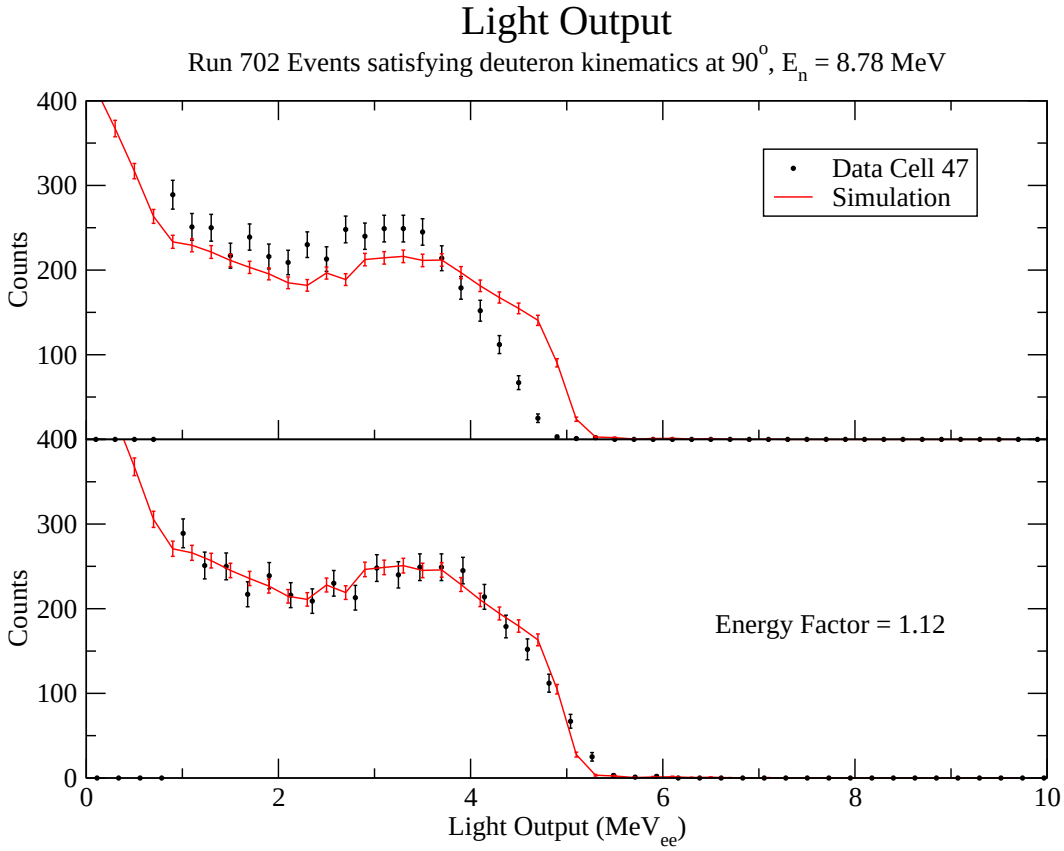

Figure 30: The light output for a cell at 90° for neutrons satisfying deuteron kinematics (i.e. with a neutron energy of 8.78 MeV) is plotted along with the simulated light output in the top graph. The lower graph shows the comparison when the light output energy scale has been multiplied by the energy factor noted.

If the light output energy scale is multiplied by a factor the agreement between the measured light output spectrum and the simulation is really quite good. This indicates that the simulation is really doing a good job of simulating the processes occurring in BC-505.

These observations are consistent with those observed by Blackston [6] and Wurtz [7].

5.2 Possible PMT Output Changes

The observations in the previous section suggest that the response of the photomultipliers is different in a data taking run, with the beam on, than it is in a calibration run, with the beam off. The simple argument against this is that if gain changes had occurred, they would be tracked by the LED/Fiber optic gain monitoring system. Indeed the gains used to produce figures 28, 29 and 30 are corrected using the flasher data. Nevertheless it would be nice to have an independent way of checking this.

The cell data in any run also includes room background. In the cell spectra for run 702 the Potassium-40 Compton edge can clearly be seen in most cells. Therefore we attempted to fit to this Compton edge in run 702 to extract a gain. Not surprisingly, the fitting algorithm had trouble with the downstream cells, but for a bit over half of the cells a gain could be extracted. These gains are on average about 5% larger than the predicted gains derived from the AmBe source run 717. However this does not take into account a possible energy offset in the gain curve. Therefore we need to first establish the gain curve at this gain setting.

Unfortunately, we only have calibration runs using the AmBe source at this gain setting of 1.67 keV/channel. Run 706 is an empty target run with beam on. In this run the cell spectra are truly dominated by room background. Therefore in this run it is possible to fit to both the Potassium-40 1.461 MeV gamma ray and the Thorium 2.614 MeV gamma ray. These two calibration points along with the AmBe 4.430 MeV gamma ray point from the calibration run 717 allow us to construct a gain curve. Such a curve is shown for one cell in figure 31. A straight line fit shows a non-zero energy offset.

From these data the gain curve slopes and offsets for all cells can be extracted. The results are shown in figure 32. Note that the offsets are smaller than that seen in figure 23 and larger than that seen in figure 25. This is consistent with the notion that larger gain offsets are present when the PMT high voltages are larger.

These results are compared in figure 32 to the slopes and offsets derived from a 2 point fit to the Potassium-40 gamma ray derived from run 702 and the gain predicted, using the flasher data, for run 702 from the AmBe run 717. This is only for cells where it was possible to fit to the Potassium-40 Compton edge in run 702. It can be seen that there is general agreement. Close agreement is not expected since the two data sets are derived from several different runs and there may have gain shift between these runs. As well, there is likely to be considerable error in simple 2 point fit used for the second data set.

The general agreement displayed in figure 32 leads us to the conclusion that the gain curve has not changed dramatically between all these data runs, which are taken under significantly different conditions: run 702 at a high data with beam on, run 706 at a low data rate (essentially room background) with beam on, and run 717 with an AmBe source and no beam.

We have re-analyzed run 702 using a gain curve that includes an offset. We have used

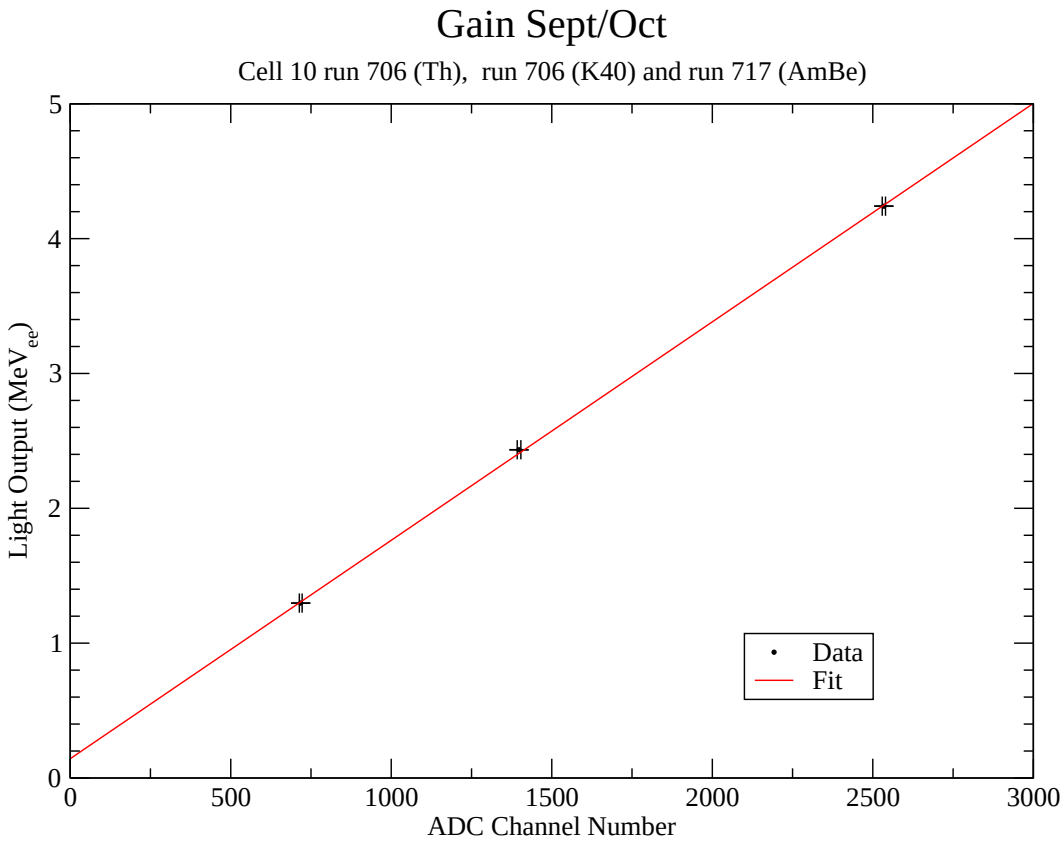

Figure 31: Energy verses channel number obtained from three data points: the 4.430 MeV AmBe gamma ray from run 717 along with the 2.614 MeV Thorium gamma ray and the 1.461 MeV Potassium-40 gamma ray from the room background in run 706. The line is the best fit straight line.

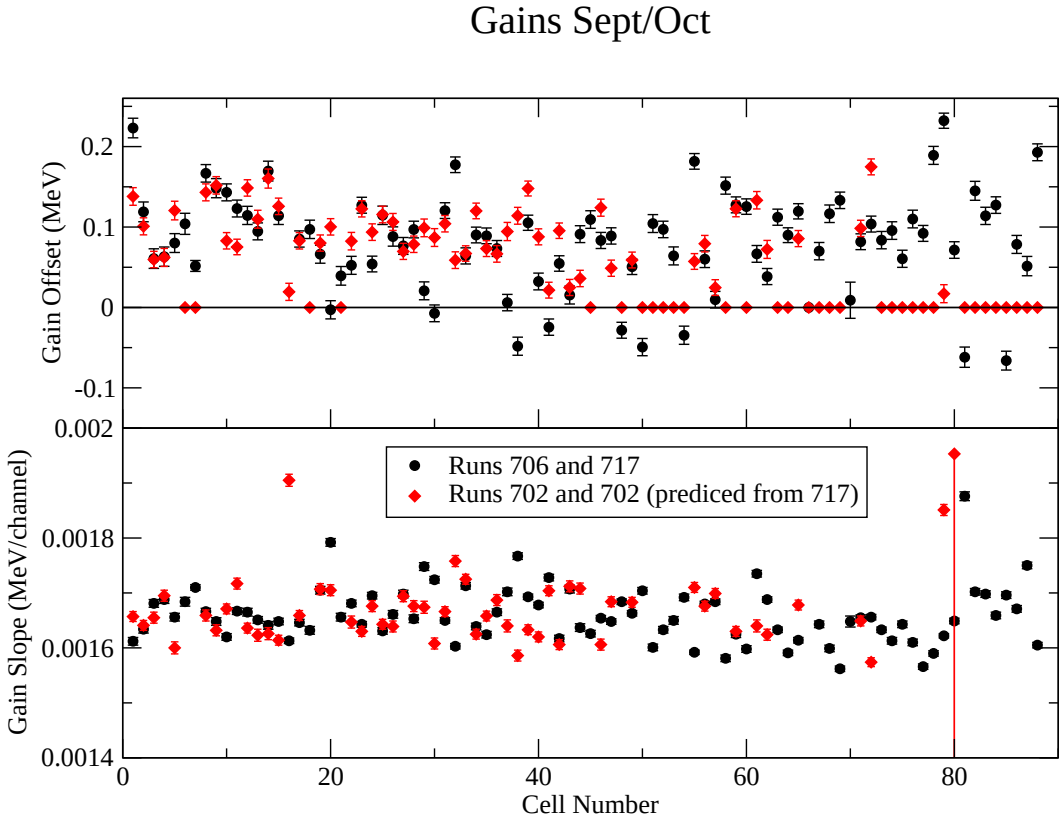

Figure 32: The fitted slopes and offsets for all cells derived from run 706 and 717 are shown by the black circles. Also shown, by the red diamonds, are the slopes and offsets obtained from a 2 point fit to the Potassium-40 gamma ray derived from run 702 and the gain predicted, using the flasher data, for run 702 from the AmBe run 717. This is only for cells where it was possible to fit to the Potassium-40 Compton edge in run 702.

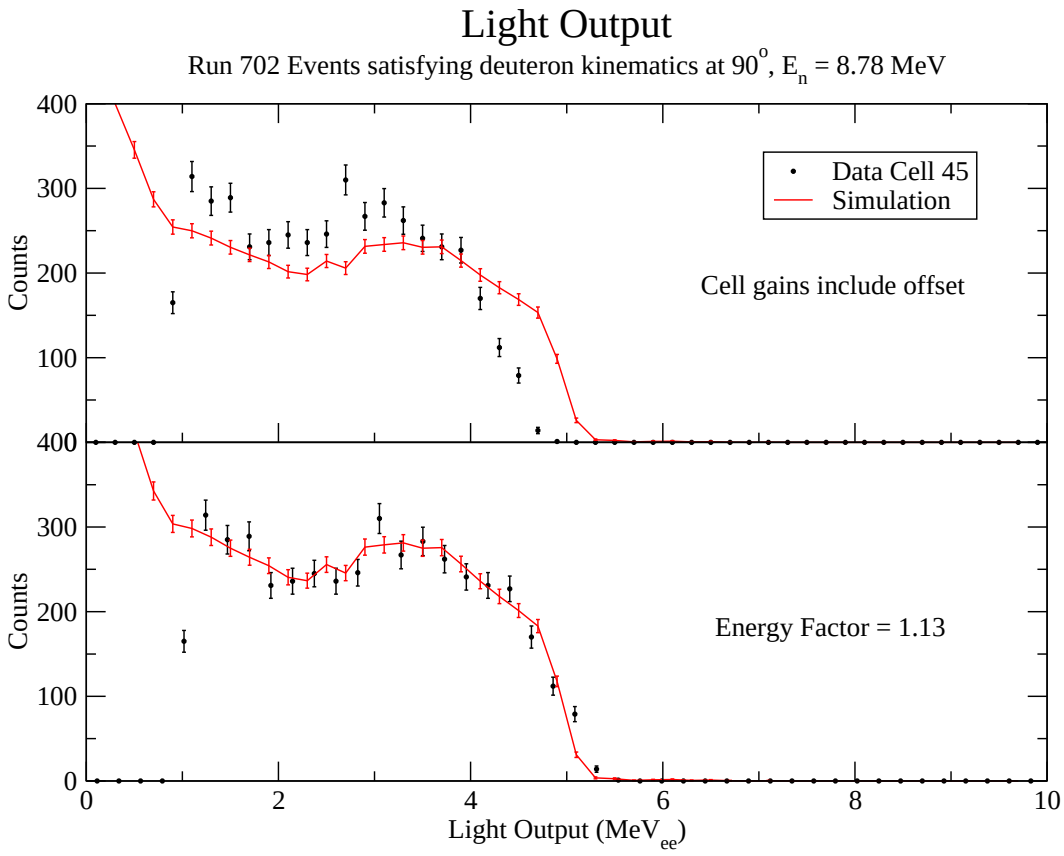

Figure 33: The light output for a cell at 90° for neutrons satisfying deuteron kinematics (i.e. with a neutron energy of 8.78 MeV) is plotted along with the simulated light output in the top graph. The gain curve used includes an offset and slope. The lower graph shows the comparison when the light output energy scale has been multiplied by the energy factor noted.

the gain slopes and offsets derived from runs 706 and 717 as a first approximation. This we think will not be a bad approximation since we see from figure 13 that there are few major changes in gain between runs 606 and 717. The light output spectrum for cell 45 is shown in figure 33. It can be seen that there is not much difference between this light output spectrum and that seen in figure 29, which ignores the offset in the gain curve. The required multiplicative factor needed to match the experimental light output spectrum to that from the simulation remains the same.

The conclusion from this section is that the detector response to *photons* does not appear to change significantly from calibration runs with no beam to data taking runs with beam on. Therefore there appears to be no significant sagging of the photomultiplier response during beam-on runs. As well, the use of a more realistic gain curve, which includes an energy offset, do not significantly change the discrepancy between the measured and simulated light output spectra for neutrons.

5.3 Light Output Discrepancy

We offer the following observations concerning this discrepancy between the observed and simulated light output spectra.

The simple answer of a mathematical error somewhere in our analysis is, while possible, we think, ruled out given that several of us have reached similar conclusions independently. Indeed, two completly independent analysis codes have been used, one based on Lucid and the other based on Root.

The light output response of BC-505 to recoil protons is unlikely to be in error. The curve agrees well with previously published data as detailed in reference [2].

The GEANT4 simulation has been able to reproduced measured light output spectra in earlier experiments as outlined in reference [2]. However, both of the experiments reported in [2] were performed with different experimental setups than the *Blowfish* configuration we are now using. The Sawatzky experiment was performed at TRIUMF using a different cell arrangement, and the Ives experiment, while it did use the *Blowfish* cell arrangement, used different electronics which included using Fastbus ADCs instead of VME ADCs. In addition, the *Blowfish* phototubes and bases have been changed since either of these experiments were performed.

The figure from reference [2] showing the comparison of the simulation with the measured light output spectrum from 8.9 MeV tagged neutrons is reproduced here as figure 34. The 8.9 MeV tagged neutrons are very close in energy to the 8.78 MeV deuteron photodisintegration neutrons we investigated in section 5.1. The simulated light output curves in figure 34 and in figures 28, 29 and 30 are very similar as expected. This indicates that there has been no unexpected change in the operation of the simulation. This suggests that the discrepancy resides with the experiment rather than the simulation.

The conclusions of section 5.2 above suggest that there is something in the current experimental set-up that makes the system response to neutron pulses different from the response to gamma ray pulses. The simple multiplicative factor needed to bring the experimental light output spectra for neutrons into line with the simulation suggests that we a missing a constant fraction of the energy in neutron pulses. The only difference between neutron and gamma ray pulses is the pulse shape. This brings us back to the idea that, because a neutron pulse is longer, we are missing more of a neutron pulse that we are missing from a gamma ray pulse (if any).

The mechanism for this missing energy is unclear. Pulse clipping from the end of the pulse would appear to be inconsistent with the conclusions of section 4.2, although those conclusions are based on an examination of gamma ray pulses only. The analysis presented in section 4.3 would seem to indicated that the effects of pulse clipping from the beginning of the pulse are not large enough to account for either the energy offset seen in the gain curves or the large light output energy error. As well, the energy offset in the gain curves is not large enough to account for the light output energy error.

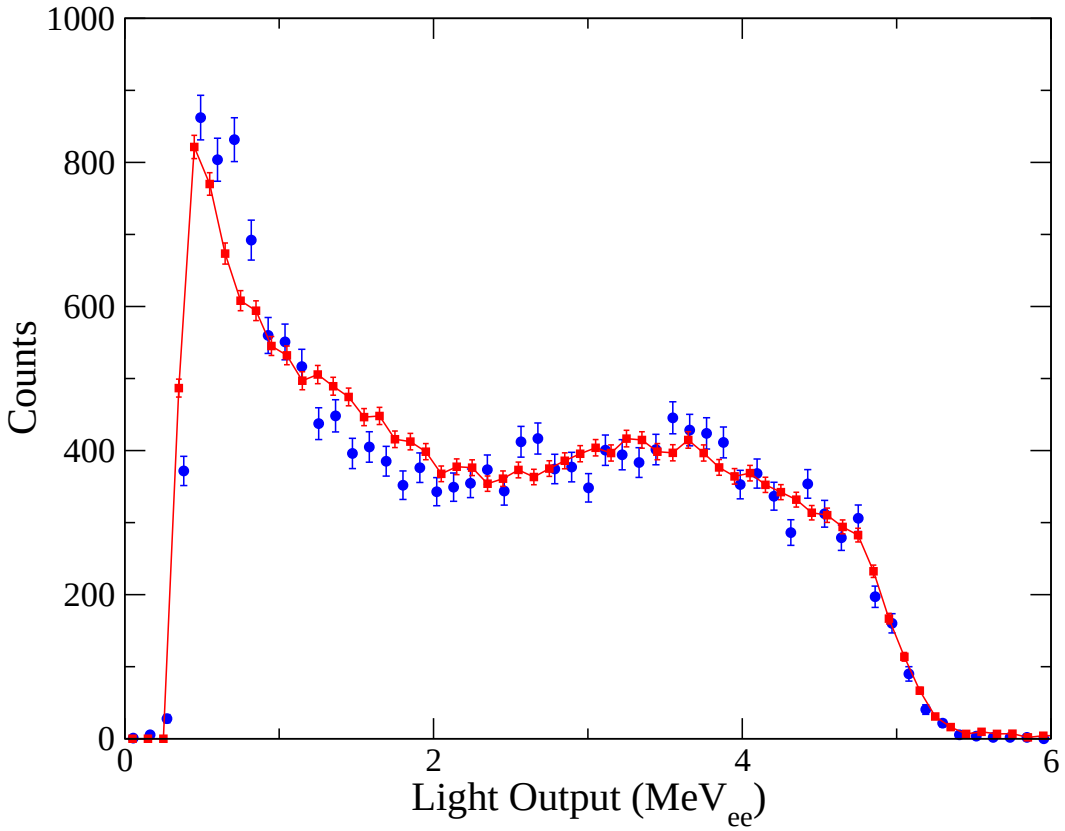

Figure 34: The light output for 8.9 MeV tagged photons compared with the GEANT4 simulation. Figure taken from reference [2].

6 Conclusions

The gain determination procedure and the operation of the flasher gain monitoring system has been examined and found to be giving good results within the limiting assumption that the gain curves are straight lines passing through the origin.

The cell gains have been shown to be better represented by a straight line that does not pass through the origin. The reason for the small energy offset has not been established.

It has been established that we are missing what appears to be a fixed fraction of the energy of neutron pulses. The reason for this has not been established. Applying a simple multiplicative factor to bring the measured neutron light output spectrum into line with a simulation appears to be justified however.

A thorough investigation of the effects of ADC gate pulse timing, gate pulse width and PMT voltage on cell gains needs to be carried out using a variety of gamma ray sources. This is needed to fully understand the BC-505 cell gain curves. While the existance of an energy offset in the gain curves is not a serious problem, it would be nice to understand its origin so that we may possibly eliminate it. The elimination of an energy offset in the gain curves will greatly simplify the gain tracking using the flasher system.

As well, a similar investigation using neutrons of known energy needs to be carried out. This is to see the effects of changing the above quantities on neutron pulses in order to understand the discrepancy between the measured neutron light output spectra and the GEANT4 simulation. The simplest way to do this would be to take data using a deuteron target.

Investigations such as these need to be carried out before any moving of the *Blowfish* electronics up to the HIGS counting room is carried out. This is because the longer cables will stretch the PMT signals and, until we understand how the pulse shapes influence the gains, we cannot predict the effects that longer pulses will have.

References

[1] G.V. O'Rielly, N.R. Kolb, and R.E. Pywell, *Nucl. Inst. and Meth. A* 368 (1996) 745.

[2] R.E. Pywell, B.D. Sawatzky, J. Ives, N.R. Kolb, R. Igarashi, and W.A. Wurtz, *Nucl. Inst. and Meth. A* 565 (2006) 725.

[3] D. Murray, et al., *LUCID User's Guide*. `http://nucleus.usask.ca/technical_reports/report_index.html`.

[4] GEANT4 Collaboration, *Nucl. Inst. and Meth. A* 503 (2003) 250.

[5] Brian Bewer, M.Sc. Thesis, *Development of a Gain Monitoring System for a Neutron Detector Array*, University of Saskatchewan, 2005.

[6] Matthew Blackston, Ph.D. Thesis, *Precision Measurements of Deuteron Photodisintegration using Linearly Polarized Photons of 14 and 16 MeV*, Duke University, 2007.

[7] Ward A. Wurtz, *Preliminary analysis of Lithium photodisintegration measurements*, Not yet published.